AD_____

Award Number: DAMD17-00-1-0443

TITLE: A Multileaf Collimator for Modulated Electron Radiation
Therapy for Breast Cancer

PRINCIPAL INVESTIGATOR: Yulin Song, Ph.D.
                         Steve B. Jiang, Ph.D.

CONTRACTING ORGANIZATION: Stanford University
                           Stanford, Californnia   94305-5401

REPORT DATE: April 2002

TYPE OF REPORT: Annual Summary

PREPARED FOR: U.S. Army Medical Research and Materiel Command
               Fort Detrick, Maryland   21702-5012

DISTRIBUTION STATEMENT: Approved for Public Release;
                        Distribution Unlimited

20020913 016

1. AGENCY USE ONLY (Leave blank)	2. REPORT DATE April 2002	3. REPORT TYPE AND DATES COVERED Annual Summary (1 Apr 01 - 31 Mar 02)

4. TITLE AND SUBTITLE

A Multileaf Collimator for Modulated Electron Radiation Therapy for Breast Cancer

5. FUNDING NUMBERS

DAMD17-00-1-0443

6. AUTHOR(S)

Yulin Song, Ph.D.
Steve B. Jiang, Ph.D.

7. PERFORMING ORGANIZATION NAME(S) AND ADDRESS(ES)

Stanford University
Stanford, Californnia 94305-5401

E-Mail: yulin@reyes.stanford.edu

8. PERFORMING ORGANIZATION REPORT NUMBER

9. SPONSORING / MONITORING AGENCY NAME(S) AND ADDRESS(ES)

U.S. Army Medical Research and Materiel Command
Fort Detrick, Maryland 21702-5012

10. SPONSORING / MONITORING AGENCY REPORT NUMBER

11. SUPPLEMENTARY NOTES
Report contains color

12a. DISTRIBUTION / AVAILABILITY STATEMENT
Approved for Public Release; Distribution Unlimited

12b. DISTRIBUTION CODE

13. ABSTRACT *(Maximum 200 Words)*

Results from recent clinical trials have shown that irradiation is an effective adjuvant therapy to lumpectomy, mastectomy, and chemotherapy for breast cancers of different stages. However, the conventional tangential photon beam treatment has two major limitations. Firstly, part of the lung and heart (in the case of the left breast treatment) may be exposed to high radiation dose. Secondly, the contralateral breast may receive a significant amount of scatter dose. Consequently, irradiation-related complications such as arm edema, myocardial infarction, severe breast fibrosis, and secondary breast cancer may occur in the patients who have undergone conventional photon beam treatment. To reduce radiation dose to normal structures and, thus, the complications, we have investigated treating breast cancers using modulated electron radiation therapy, making use of the rapid depth dose falloff characteristics of electron beams. To deliver MERT plans effectively, we designed and manufactured a prototype electron multileaf collimator based on the results of Monte Carlo simulations. The performance of the EMLC was experimentally evaluated and the results were compared with those of Monte Carlo simulations. Our results showed that there was an excellent agreement between the film measurements and the Monte Carlo simulated data at all electron energies in terms of dose distribution.

14. SUBJECT TERMS
Modulated Electron Radiation Therapy (MERT), Multileaf Collimator (MLC), Electron Multileaf Collimator (EMLC).

15. NUMBER OF PAGES
44

16. PRICE CODE

17. SECURITY CLASSIFICATION OF REPORT Unclassified	18. SECURITY CLASSIFICATION OF THIS PAGE Unclassified	19. SECURITY CLASSIFICATION OF ABSTRACT Unclassified	20. LIMITATION OF ABSTRACT Unlimited
Unclassified	Unclassified	Unclassified	Unlimited

Table of Contents

1. INTRODUCTION

This **Postdoctoral Traineeship** has two primary goals. The first one is to provide the PI with a good opportunity to learn and apply modern radiotherapy techniques to breast cancer treatment and to train the PI for a career as a breast cancer research scientist and a radiation oncology physicist. The second goal is to simulate, design, manufacture, and evaluate an electron multileaf collimator (EMLC) specifically for energy- and intensity-modulated electron radiation therapy. Because the original PI, Dr. Steve B. Jiang, left Stanford University School of Medicine in September, 2000, Stanford University, with the approval of the U.S Army Medical Research Acquisition Activity (USAMRAA), transferred the PIship to me on January 17, 2002. As a result, my mentor, Dr. Arthur Boyer, requested the U.S. Army to extend the term of the **Traineeship** for one more year without additional funds. The request was approved by the USAMRAA on March 24, 2002. In this report, I will summarize the highlights of my past year's training and research as originally proposed in the **Postdoctoral Traineeship** application.

2. BODY

Training

The Department of Radiation Oncology at Stanford University School of Medicine has established a comprehensive postdoctoral training program in radiation physics for many years. The program emphasizes not only the cutting-edge research related to radiation therapy, computer simulation and modeling, image processing, and molecular imaging, but also provides extensive clinical training to its postdoctoral fellows, ranging from the state of the art intensity modulated radiation therapy (IMRT) to frameless radiosurgery. Under the leadership of Dr. Arthur Boyer, the Director of the Radiation Physics Division, this program has undergone major changes in terms of clinical training. It has now become one of the best postdoctoral training programs in radiation physics in the United States. Last year, the Department of Radiation Oncology offered two courses to its radiation oncology residents and postdoctoral fellows: the Physics of Radiation Therapy and Radiobiology. Both courses were one-semester long and covered the major aspects of radiation physics and radiobiology with emphasis on the practical details. In addition, the Department also held its annual IMRT Symposium and AcQSim Symposium, which all postdoctoral fellows were required to attend. AcQSim is a software

package for optimizing CT-based localization and treatment planning. The Department of Radiation Oncology also had weekly clinical radiation physics seminars, in which guess speakers, faculty, and postdoctoral fellows presented their research results. Under the direct guidance of Dr. Arthur Boyer, I have learned the basic theories of Monte Carlo simulation, modulated electron radiation therapy (MERT), intensity modulated radiation therapy (IMRT), and sweeping window arc therapy (SWAT). I have also learned how to operate Varian CLINAC linear accelerators (Varian Medical Systems, Palo Alto, CA) and Wellhöfer dosimetry data acquisition system. In addition, I have also learned film dosimetry and commissioning of radiation treatment planning (RTP) system. As an important part of my postdoctoral training, I was also assigned clinical duties such as IMRT treatment planning, chart check, and machine QA.

Research

Results from recent clinical trials have shown that irradiation is an effective adjuvant therapy to lumpectomy, mastectomy, and chemotherapy for breast cancers of different stages [1, 2]. However, the conventional tangential photon beam treatment has two major limitations. Firstly, part of the lung and heart (in the case of the left breast treatment) may be exposed to high radiation dose. Secondly, the contralateral breast may receive a significant amount of scatter dose. Consequently, irradiation-related complications such as arm edema, myocardial infarction, severe breast fibrosis, and secondary breast cancer may occur in the patients who have undergone conventional photon beam treatment [3-5]. To reduce radiation dose to normal structures and, thus, the complications, we have investigated treating breast cancers using modulated electron radiation therapy (MERT) [6, 7], making use of the rapid depth dose falloff characteristics of electron beams. To deliver MERT plans effectively, we designed and manufactured a prototype electron multileaf collimator (EMLC). The performance of the EMLC was experimentally evaluated and the results were compared with those of Monte Carlo simulations.

Monte Carlo simulations were carried out on a cluster of 22 Pentium Pro CPUs (200 MHz) and 10 Pentium III CPUs (450 MHz), all running EGS4/BEAM, MCDOSE and their utilities under the Linux operating system. Based on the manufacturer's specifications of the beam production system and the EMLC design, the electron beams were simulated using the

EGS4/BEAM code All simulation parameters, such as the electron and photon energy cutoffs (ECUT and PCUT), the maximum fractional energy loss per electron step (ESTEPE), and the number of initial electron histories were specified in the EGS4/BEAM input file. In this study, we used ECUT = 700 KeV and PCUT = 10 KeV, below which all remaining energy was deposited on the spot. It has been shown that an ECUT of 700 KeV, corresponding to a residual continuous-slowing-down approximation (CSDA) range in water of < 0.5 mm, is sufficient for most dosimetric purposes [8]. ESTEPE was set to 0.04 and PRESTA (parameter reduced electron step algorithm) for extensions were used for step length calculations [9]. The EMLC was included in the EGS/BEAM simulations as an MLC component module. The number of initial electron histories ranged from 150×10^6 for 6 MeV to 50×10^6 for 20 MeV. Phase space data were scored at a plane of 100 cm source-surface distance (SSD) after the particles had transported through the linac treatment head, the EMLC, and the air gap beneath it. The phase space data were then analyzed using BEAMDP code [10] to obtain the electron fluence profiles at different depths for different energies. Based on the phase space data, dose distributions in a homogenous water phantom with each voxel size of $3 \times 15 \times 2$ mm^3 were computed using the EGS4/MCDOSE code [11].

Based on the results of our Monte Carlo simulations, an experimental EMLC was fabricated by modifying a conventional 25×25 cm^2 electron cone donated by Varian Medical Systems (Palo Alto, CA). The EMLC consisted of 30 steel leaf pairs, with each leaf being 0.476 cm wide, 20.0 cm long, and 2.54 cm thick. Both sides and ends of the leaves were made parallel with the central beam axis. The maximum opening was 14.2×15.5 cm^2 when all leaves were completely retracted, giving the largest radiation field of 15.0×16.3 cm^2 projected at 100 cm SSD. The leaves can move freely along the x direction, *i.e.* from patient right to left. For each of the beam segments, the corresponding field shape was obtained by manually positioning the leaves according to their coordinates computed from our electron beam leaf-sequencing program. To set the field shape more efficiently, currently, we first drew the field shape on a piece of hard cardboard at a ratio of 1:1 and cut it out. The field shape was then set using this pre-cut cardboard. In the near future, we will develop a faster and more accurate way of setting field shapes. Because the EMLC was used, the electron cutout that was originally inserted in the last scraper of the electron cone was no longer needed. Therefore, we removed the last scraper and its

electronic circuitry and the EMLC was placed immediately at the bottom of the modified electron cone and stabilized with eight screws. This modification resulted in a much smaller air gap (5.0 cm) between the bottom of the EMLC leaves and the patient skin and thus, reduced air scattering effect. To avoid activating interlocks associated with electron beam accessory malfunction while inserting the EMLC into the linac treatment head, we also modified the coding of the electron cone. Figure 1 shows a photo of the EMLC inserted on the treatment head of a Varian CLINAC 2100C linear accelerator.
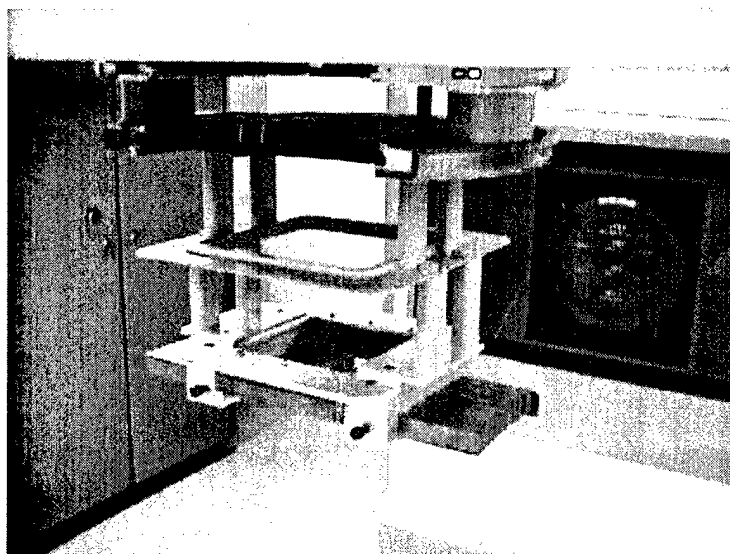
Figure 1 A photo of the prototype EMLC.

Film (Kodak X-omat V, Eastman Kodak Company, Rochester, NY) dosimetry of the prototype EMLC was performed on a Varian CLINAC 2100C linear accelerator. Measurements were taken at energies of 6, 12, and 20 MeV and at the surface, 1.5 and 3.0 cm depths in a solid water phantom to evaluate the quality of the electron beams collimated by the EMLC. The films were scanned using a VXR-12 PLUS film digitizer (VIDAR Systems Corporation, Herndon, VA) and calibrated according to the AAPM TG-25 recommendations. Dose distributions, flatness and symmetry, and the extent of the beam penumbra were accessed using the RIT113 radiation therapy film dosimetry system (Radiological Imaging Technology, Colorado Springs, CO) and compared with the simulated dose results. Our results showed that there was an excellent agreement between the film measurements and the Monte Carlo simulated data at all

electron energies in terms of dose distribution. We found that the EMLC provided significant improvements in dose penumbras and field resolution as compared to the photon MLC. We also found that MERT was able to provide similar or better target dose coverage compared with x-ray IMRT. However, MERT could significantly reduce the dose to critical structures.

3. KEY RESEARCH ACCOMPLISHMENTS

- Designed and fabricated an experimental EMLC by modifying a conventional 25 x 25 cm^2 electron cone donated by Varian Medical Systems for MERT plan delivery.

- Performed film dosimetry to experimentally evaluate the quality of the EMLC in terms of dose distribution, flatness and symmetry, and the extent of the beam penumbra.

- Incorporated the EMLC into the EGS/BEAM simulations as an MLC component module and created some MERT plans for breast cancers.

4. REPORTABLE OUTCOMES

----PUBLICATIONS:
Manuscript
1. Michael C. Lee, Jun Deng, Jinsheng Li, **Steve B. Jiang**, and C-M. Ma, "Monte Carlo based treatment planning for modulated electron radiotherapy", *Phys. Med. Biol.* **46**:(2001) 2177-2199.

Abstracts
1. **Yulin Song**, Michael C. Lee, and Arthur L. Boyer, "Energy and intensity modulated electron radiotheray: A comparative dosimetric study of MERT and IMRT for head & neck cancer", To be presented at the 44th Annual Meeting of the American Association of Physicists in Medicine, Montreal, Canada, July 18-21, 2002.

2. Gary Luxton, **Yulin Song**, Jenny Hai, and Arthur L. Boyer, "TLD measurement system for comprehensive dosimetric quality assurance in IMRT", To be presented at the 44th Annual

Meeting of the American Association of Physicists in Medicine, Montreal, Canada, July 18-21, 2002.

3. Arthur L. Boyer, **Yulin Song**, Yong Yang, and Lei Xing, "Sweeping window arc therapy", To be presented at the 44th Annual Meeting of the American Association of Physicists in Medicine, Montreal, Canada, July 18-21, 2002.

4. Bilal Shahine, **Yulin Song**, David Findley, C-M Ma, Arthur L. Boyer, and Todd Pawlicki, "Commissioning of Multigrid Superposition algorithm for IMRT treatment planning", Submitted for the 44th Annual Meeting of the American Society for Therapeutic Radiology and Oncology (ASTRO), New Orleans, LA, USA, October 6-10, 2002.

5. **Yulin Song**, Jun Lian, and Lei Xing, "Inclusion of biological parameter uncertainty in the treatment planning optimization", Submitted for the 44th Annual Meeting of the American Society for Therapeutic Radiology and Oncology (ASTRO), New Orleans, LA, USA, October 6-10, 2002.

6. **Yulin Song**, Steve B. Jiang, Michael C. Lee, C-M Ma, and Arthur L. Boyer, "A multileaf collimator for modulated electron radiation therapy (MERT) for breast cancer", Submitted for the Era of Hope 2002 DoD Breast Cancer Research Program Meeting, Orlando, Florida, USA, September 25-28, 2002.

7. Lei Xing, Jonathan G. Li, **Yulin Song**, David Y. Yang, Don Goffinet, and Arthur L. Boyer, "Combining electron with intensity modulated photon beams for breast cancer", Submitted for the Era of Hope 2002 DoD Breast Cancer Research Program Meeting, Orlando, Florida, USA, September 25-28, 2002.

----EMPLOYMENT RECEIVED ON TRAINING SUPPORTED BY THIS POST-DOCTORAL TRAINEEWSHIP:
Steve B. Jiang, Ph.D., Assistant professor, the Department of Radiation Oncology, Massachusetts General Hospital, Harvard Medical School, Boston, MA.

5. CONCLUSIONS

Based on the results of our Monte Carlo simulations, we conclude that EMLC was able to provide sufficient beam collimation for MERT and Monte Carlo simulation provides an accurate technique for computing dose distributions from such a beam collimation system.

6. REFERENCES

[1] Solin, LJ, Kurtz, J, and Fourquet, A., et al, "Fifteen years results of breast-conserving surgery and definitive breast irradiation for the treatment of ductal carcinoma in situ of the breast", *J. Clin. Oncol.*, **14**:754-763, 1996.

[2] Fisher, B, Dignam, J, and Wolmark, N, et al, "Lumpectomy and radiation therapy for the treatment of intraductal breast cancer: findings from National Surgical Adjuvant Breast and Bowel Project B-17", *J. Clin. Oncol.*, **16**:441-452, 1998.

[3] Boice Jr, JD, Harvey, EB, and Blettner, M, et al., "Cancer in the contralateral breast after radiotherapy for breast cancer", *N. Engl. J. Med.*, **326**:781-785, 1992.

[4] Gyenes, G, Rutqvist, LE, Liedberg, A, and Fornander, T, "Long-term cardiac morbidity and mortality in a randomized trial of pre-and postoperative radiation therapy versus surgery alone in primary breast cancer ", *Radiother. Oncol.* **48**:185-190, 1998.

[5] Lingos, TI, Recht, A, and Vicini, F, et al, "Radiation pneumonitis in breast cancer patients treated with conservative surgery and radiation therapy", *Int. J. Radiat. Oncol. Biol. Phys.* **21**:355-360, 1991.

[6] Ma, C-M, Mok, E, Kapur, A, Pawlicki, T, Findley, D, Brain, S, Forster, K, and Boyer, AL, "Clinical implementation of a Monte Carlo treatment planning system", *Med. Phys.*, **26**:2133-2143, 1999.

[7] Ma, C-M, Pawlicki, T, Lee, MC, Jiang, SB, Li, JS, Deng, J, Mok, E, Yi, B., Luxton, G, and Boyer, AL, "Energy- and intensity-modulated electron beams for radiotherapy", *Phys. Med. Biol.*, **45**:2293-2311, 2000.

[8] Rogers, DWO, Faddegon, BA, Ding, GX, Ma, C-M, Wei, J, and Mackie, TR, "BEAM: A Monte Carlo code to simulate radiotherapy treatment units", *Med. Phys.*, **22**:503-524, 1995.

[9] Bielajew, A, and Rogers, DWO, "PRESTA - the parameter reduced electron step algorithm for electron Monte Carlo transport", *Nucl. Instrum. Methods Phy. Res.*. **18**:165-181, 1987.

[10] Ma, C-M, and Rogers, DWO, "BEAMDP Users Manual", *National Research Council Report No. PIRS*-0509(C), NRC, Ottawa, Canada, 1995.

[11] Ma, C-M, Li, JS, Pawlicki, T, Jiang, SB, and Deng, J, "MCDOSE - A Monte Carlo dose calculation tool for radiation therapy treatment planning", *Proceedings of the XIII International Conference on the Use of Computers in Radiotherapy*, edited by Schlegel, W, and Bortfeld, T (Springer, Heidelberg, Germany), pp. 123-125.

7. APPENDICES

Copies of manuscripts and abstracts

Monte Carlo based treatment planning for modulated electron beam radiation therapy

Michael C Lee, Jun Deng, Jinsheng Li, Steve B Jiang[1] and C-M Ma

Radiation Physics Division, Department of Radiation Oncology,
Stanford University School of Medicine, Stanford, CA 94305-5304, USA

E-mail: mclee@reyes.stanford.edu

Abstract

A Monte Carlo based treatment planning system for modulated electron radiation therapy (MERT) is presented. This new variation of intensity modulated radiation therapy (IMRT) utilizes an electron multileaf collimator (eMLC) to deliver non-uniform intensity maps at several electron energies. In this way, conformal dose distributions are delivered to irregular targets located a few centimetres below the surface while sparing deeper-lying normal anatomy. Planning for MERT begins with Monte Carlo generation of electron beamlets. Electrons are transported with proper in-air scattering and the dose is tallied in the phantom for each beamlet. An optimized beamlet plan may be calculated using inverse-planning methods. Step-and-shoot leaf sequences are generated for the intensity maps and dose distributions recalculated using Monte Carlo simulations. Here, scatter and leakage from the leaves are properly accounted for by transporting electrons through the eMLC geometry. The weights for the segments of the plan are re-optimized with the leaf positions fixed and bremsstrahlung leakage and electron scatter doses included. This optimization gives the final optimized plan. It is shown that a significant portion of the calculation time is spent transporting particles in the leaves. However, this is necessary since optimizing segment weights based on a model in which leaf transport is ignored results in an improperly optimized plan with overdosing of target and critical structures. A method of rapidly calculating the bremsstrahlung contribution is presented and shown to be an efficient solution to this problem. A homogeneous model target and a 2D breast plan are presented. The potential use of this tool in clinical planning is discussed.

1. Introduction

In an increasing number of centres, the treatment of tumours in close proximity to critical organs or targets possessing complex geometries is performed via intensity modulated radiation therapy (IMRT) with photon beams. While this technique is an extremely powerful tool for treating tumours that are located more than a few centimetres below the surface, the physics of x-ray energy deposition suggests that photon IMRT is not well suited to the treatment of shallow targets. Furthermore, in many cases the slow attenuation of photon beams makes conventional photon IMRT a poor choice for some targets with distal critical structures. In contrast, electron beams, with their comparatively higher surface doses and more rapid depth–dose fall-offs, are well suited to these targets. However, conventional electron beam delivery and treatment planning systems are ill-equipped for the delivery of complex dose distributions.

Modulated electron beam radiation therapy (MERT) is a new electron modality that has been developed to deliver highly conformal doses to shallow targets (Lief *et al* 1996, Hyödynmaa *et al* 1996, Zackrisson and Karlsson 1996, Åsell *et al* 1997, Ebert and Hoban 1997, Karlsson *et al* 1998, 1999, Åsell *et al* 1999, Ma *et al* 2000b). Dose conformality in the beam direction may be achieved by energy modulation, while lateral uniformity and conformity may be achieved by intensity modulation via a variable collimator. Many of the studies into MERT have used microtron based scanned beam systems. In principle, energies should be selectable with relative ease on these systems, while intensity modulation could be achieved by scanning the narrow electron beam. Studies using these systems have shown MERT to be feasible and potentially of great value; however, the cost and availability of such machines have greatly restricted research and development of scanned beam based MERT. Investigations into the use of the photon MLCs on accelerators that broaden electron beams with scattering foils have also been performed, including the possibility of using helium along the beam axis to reduce deleterious air scatter (Karlsson *et al* 1999, Lee *et al* 2000a).

As an alternative to these systems, an electron-specific multileaf collimator (eMLC) has been proposed (Lee *et al* 2000a, Ma *et al* 2000b). It has been demonstrated that a collimator consisting of 1.5 cm thick tungsten leaves located at the level of the last scraper of a 25×25 cm^2 electron applicator allows shaping of the field to a higher degree of resolution than is possible using the photon MLC. By superposition of a number of different field shapes, an intensity modulated field may be delivered. However, a system for generating such a plan required further research.

Any planning system requires the ability to perform accurate dose calculations. Because electron transport and scatter in matter is strongly influenced by density and material composition, dose calculation in heterogeneous media is extremely challenging. Conventional algorithms typically utilize variants of the 3D Hogstrom pencil beam algorithm, based on Fermi–Eyges transport theory (Hogstrom *et al* 1981). However, it has been well documented that in heterogeneous phantoms and small irregular fields, this algorithm results in large regions of dose error (Cygler *et al* 1987, Bielajew *et al* 1987, Mah *et al* 1989, Mackie *et al* 1994, Ma *et al* 1999). It has been demonstrated that the Monte Carlo method can provide accurate dose estimations under all circumstances (Cygler *et al* 1987, Mackie *et al* 1994, Kawrakow *et al* 1996, Mohan 1997, Kapur 1999, Ma *et al* 1999). Additionally, Monte Carlo transport algorithms can be used to accurately assess the perturbations to the electron fluence caused by beam modifiers, such as multileaf collimators (assuming an accurate source model). The combined effects of field size, shape, and collimator on absolute doses can then be included as planning considerations with a high degree of accuracy. Thus, while the need for Monte Carlo dose computation of photon IMRT plans has been debated, the importance of Monte Carlo in conventional electron plans is well established, and it follows that more complex MERT plans will also benefit from Monte Carlo computation.

Most photon IMRT planning systems divide a radiation field into small spatial elements, or beamlets, and separate out the dose contribution from each beamlet as the first step in planning. This beamlet simulation may be performed by analytical methods or by the Monte Carlo method (Boyer and Mok 1985, Pawlicki *et al* 1999, Laub *et al* 2000). By optimizing on the dose distributions, weights or intensities for each beamlet may be obtained and the resulting 2D intensity maps may be converted into an MLC leaf sequence for delivery. The assumption is that the dose computed on a beamlet-by-beamlet basis is the same as the dose delivered via the actual leaf sequence. Even in photon IMRT this is not the case, the MLC tongue-and-groove effect being the most notable violation (van Santvoort *et al* 1996, Yu 1998), with transmission through leaf ends and edges also being a factor (Chen *et al* 2000). In these instances, an additional correction must be applied to leaf sequences or simply during dose reconstruction so that planners may evaluate the true dose rather than an ideal dose.

This difference between beamlet and delivered doses is the primary challenge encountered in developing a MERT planning system. During delivery, electrons (and contaminant photons) have the opportunity to scatter off or through leaf ends and sides to a much greater degree than photons. Additionally particles incident on the closed portions of the leaves may generate secondary particles, in particular bremsstrahlung photons (Lee *et al* 2000a). These effects result in a leaf-delivered dose that may differ significantly from the beamlet predicted dose. The magnitude of this effect depends on the specific plan and cannot be known *a priori*.

Holmes (2001) has proposed a tomotherapy planning system that accounts for aperture-dependent non-idealities such as leakage and head scatter. In that system, leaf sequencing occurred as part of the optimization procedure, and thus aperture-dependent leakage and head scatter could be included for each 'field' delivered by the tomotherapy system. This work seeks to apply the same concept to MERT planning, though in this case Monte Carlo calculated aperture-dependent non-idealities are incorporated via a *post hoc* procedure rather than during the optimization.

The objective of this study was first to examine the differences between beamlet deliveries and dose distributions from simulations in which particles were transported in the eMLC. A Monte Carlo based treatment planning system was then developed in which the bremsstrahlung leakage and leaf-end scatter and transmission could be properly accounted for in the optimization process. A method of implicitly including the effect of particle transport in the leaves was developed, allowing for faster calculations. Using this system, a plan is generated for an artificial homogeneous phantom and for a CT phantom of an intact breast. Based on these results, potential directions for further research are discussed.

2. Methods

2.1. Monte Carlo simulations

Source parameter descriptions of 6, 9, 12, 16 and 20 MeV (nominal energy) electron beams were obtained using a procedure described elsewhere and summarized here. Electron beam simulations of a Varian Clinac 2100C (Varian Oncology Systems, Palo Alto, CA) were performed using the EGS4/BEAM code (Nelson *et al* 1985, Rogers *et al* 1995). A 25×25 cm^2 type III (open walled) applicator was used in these simulations. Vendor supplied geometries were used to define the component modules in the BEAM simulation, with photon jaw settings adjusted according to the nominal beam energy. It has been shown elsewhere that the resulting phase space data from these simulations, when used in EGS4/DOSXYZ or MCDOSE dose calculations, provide agreement with measured data to within 2% on depth-dose and transverse profiles, as well as output factor calculations (Kapur *et al* 1998, Kapur 1999, Lee *et al* 2000c).
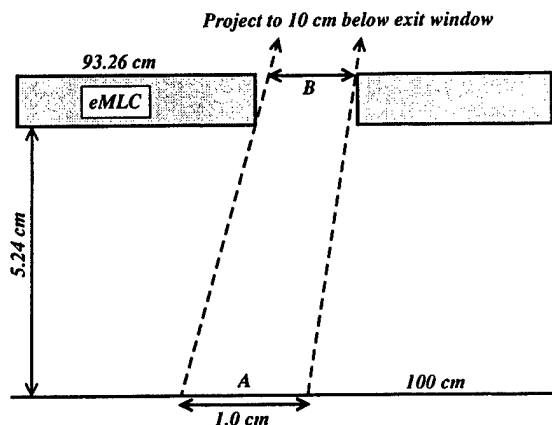
Figure 1. A schematic diagram of the beamlet and electron MLC geometry. The beamlet is defined as having a width of exactly 1.0 cm at 100 cm from the photon target, regardless of where the phantom surface is actually located. This is shown in A. The source plane is reconstructed at 93.26 cm, coincident with the upper surface of the eMLC. The beamlets are then defined at this plane B by ray tracing from the approximate location of the electron virtual source, 10 cm below the exit window. Only particles within B are reconstructed and beamlet simulation occurs without any collimation. When leaves are simulated, their positions are set based on the geometric projections of the leaf edges, as shown. Thus there is an inherent difference in beamlet simulation and actual delivery.

During the simulation, 'latch bit' settings were used to delineate particles originating or scattering off the first two scrapers of the applicator (source 1 and 2), and electrons (source 3) and photons (source 4) that were well described by a virtual point source (Ma *et al* 1997, Ma and Rogers 1997, Jiang *et al* 2000). This four-source model has been shown to provide agreement with both the direct phase-space simulation and measured data (Jiang *et al* 2000). During dose calculations particles were generated according to this source model, thus eliminating the need for calculation and storage of large phase-space data files.

Unless otherwise noted, electrons were transported down to 0.70 MeV total energy (ECUT) and photons transported to 10 keV energy (PCUT), at which point the remaining energy was deposited on the spot. It has been documented that an ECUT of 0.70 MeV, corresponding to a residual continuous slowing down approximation range in water of <0.5 mm, is sufficient for most dosimetric purposes (Rogers *et al* 1995). Transport through the leaves and in air was performed using PRESTA for step-length calculations (Bielajew and Rogers 1987). For transport in the phantom, photon splitting and electron track repetition were employed as variance reduction techniques (Kawrawkow and Fippel 2000, Ma *et al* 2000a).

Dose calculations were performed using the EGS4 user code MCDOSE (Nelson *et al* 1985, Ma *et al* 2000a). This code has been described in detail elsewhere and has been shown to provide agreement with DOSXYZ and measured data to within 2% (Li *et al* 2000b). The code was modified and used for MERT planning as described in the following sections.

2.1.1. Electron beamlets. For each energy and port, electron beamlets were simulated for use in the inverse planning algorithm in a manner analogous to Monte Carlo based photon IMRT planning (Pawlicki *et al* 1999). Beamlet size was set at the level of isocentre, with a resolution of 1 cm. The beamlet was then defined by a virtual aperture located at the position of the upper surface of the electron MLC, 93.26 cm below the photon target. The beamlet size was defined

to be given by projections taken from the plane containing the isocentre to the approximate location of the electron virtual source, 10 cm below the photon target as determined during beam commissioning. This geometry is shown schematically in figure 1. The virtual aperture could be simulated in one of two ways:

(a) By taking the beamlet to be an opening in a perfectly absorbing infinitely thin collimator, that is, sampling from the full 25×25 cm^2 field and transporting only those particles that land in the beamlet.

(b) Sampling directly within the beamlet itself, and never generating any particles in the remaining regions.

For efficiency, method (b) was selected with weighting factors defined as follows.

Let us consider a subset of a two-dimensional fluence profile ('beamlet') defined by $x = x_1$ to x_2 and $y = y_1$ to y_2 with area $A_{beamlet}$. If we sample within this beamlet according to the true distribution, then each particle can be given a weighting factor equal to the ratio of the integral fluence within the beamlet to the overall integrated fluence. If, however, we sample *uniformly* within this region, then we must apply an additional weighting factor to remove the biasing due to the uniform sampling. If the intensities (number of particles in a bin) are given as $F(x, y)$ and we consider a point (x', y'), then

$$w(x', y') = \frac{A_{beamlet}}{A_{bin}} \frac{F(x', y')}{\sum_x \sum_y F(x, y)} \tag{1}$$

where A_{bin} is the area of the spatial bin to convert number of particles to fluence and the summation represents the total number of particles in the source parameter file.

As mentioned above, each source parameter file contains fluence information for four subsources. Because spatial bins are defined in the same way for each subsource, it is possible to assign a cumulative distribution function (CDF) for each bin, describing the relative intensities of each source. Particles are sampled according to this CDF and hence no additional weighting factor is needed for subsources. Note that contaminant photons from the treatment head are included in the source reconstruction during both beamlet and eMLC simulation. Particle origins are uniformly sampled on each subsource (i.e. an electron has an equal probability of coming from each edge of an electron scraper). The reader is referred to Jiang *et al* (2000) for complete details on source reconstruction for this four-source model, with the aforementioned weighting factors for beamlet sampling.

During beamlet simulation, particles are reconstructed at the upper surface of the eMLC at a distance 93.26 cm below the nominal photon target position. The remaining air gap to the phantom is then explicitly simulated, thus accounting for the in-air scatter, such that the final fluence at the phantom surface is essentially a convolution of the original fluence and the scatter kernel.

2.1.2. Electron MLC simulation. A proposed design for an electron specific MLC (eMLC) has been described elsewhere and is summarized below (Lee *et al* 2000a). Based on measurements with a prototype system and Monte Carlo simulations, it has been shown that 1.5 cm thick tungsten leaves located at the level of the last scraper provide adequate electron collimation for MERT. Leaf ends and sides may be unfocused, though in this study leaf sides were considered to be focused to a point 10 cm below the photon target (for the 2D targets studied here, this has no significant effect). Note that while this study utilized this specific eMLC design, the results are general to any collimator in which leaf end scatter and transmission and bremsstrahlung leakage are non-trivial.

The MCDOSE code was modified to include the simulation of particle transport in such a collimator, placed according to arbitrary table, collimator and gantry angles, with leaves set

according to a leaf sequence file. The geometry coding routines were based upon macros used for block simulations (Li *et al* 2000a, b). In all simulations, a region extending from the field edge 5 mm into the leaves of the eMLC was subject to explicit simulation of all particles, up to the global transport cut-offs. Margins of thickness greater than 3 mm have been shown to be adequate for accounting for edge effects in cut-outs (Mubata *et al* 2000). Outside this region, one of two rejection methods was used to accelerate the simulations. In one method all particles in this region were rejected, while in the second method electrons were discarded based on a 2 MeV total energy cut-off while photons were transported explicitly. An alternative method for computing bremsstrahlung leakage was investigated and is described separately in section 2.1.3.

Each segment of the MERT plan was given a different number of histories based upon the number of monitor units to be delivered. Note, however, that the absolute dose is decoupled from the number of histories delivered, because the absolute dose for each field is separately computed assuming a single monitor unit delivery, and then rescaled to the correct value. However, for increased speed, the number of particles simulated was proportional to the number of MU to be delivered. In particular, the overall statistical uncertainty at a point after N segments with relative intensities w is given by

$$\sigma_{\text{tot}}^2 = \sum_{i=1}^{N} (w_i \sigma_i)^2. \tag{2}$$

If we express all the intensities in units of the minimum intensity, w_{min}, such that $w_i = \alpha_i w_{\text{min}}$, we may write

$$\sigma_{\text{tot}}^2 = \sum_{i=1}^{N} (\alpha_i^2 w_{\text{min}}^2 \sigma_i^2). \tag{3}$$

If we desire to have all segments provide an equal contribution to the overall uncertainty, then $(\alpha_i^2 \sigma_i^2)$ must stay constant over i. This implies that the square of the uncertainties should scale linearly with the square of the intensities, or equivalently, the number of histories for a field should scale with the square of the intensities. The uncertainty in the final plans was less than 1% at 1σ for the voxels with a dose $D > 0.5 D_{\text{max}}$. By using a low uncertainty (at the cost of high computation time), the noise-convergence issue of Monte Carlo based inverse planning can be minimized (Jeraj and Keall 2000, Keall *et al* 2000).

2.1.3. Bremsstrahlung background approximation. In a subset of the simulations, leakage photons were included in the calculations without explicit transport through the leaves. Using the EGS4/BEAM system, two phase space files were generated, one directly above and one directly below a 1.5 cm tungsten slab. Only particles passing through a 10×10 cm^2 square centred on the slab's upper surface were transported and scored. The photons in the lower phase space were placed into angular bins of 1.0° (taken with respect to the central axis) and within each angular bin, particles were separated into energy bins of 0.5 MeV. A 'total photon yield' S was defined as the number of photons in the lower phase space divided by the total number of particles in the upper phase space. Note that this differs from the standard definition of bremsstrahlung yield in that all photons are scored including, for example, transmission, rather than only bremsstrahlung, and the yield is given per incident particle rather than per incident electron.

The Monte Carlo simulation employed the bremsstrahlung production cross sections of Koch and Motz (1959). The validity of the Monte Carlo method for studying thick-target bremsstrahlung has been discussed at length in the literature (e.g. Seltzer and Berger 1985, Faddegon *et al* 1990, 1991).

During source reconstruction, electrons that would be incident upon the upper surface of the eMLC are discarded (recall that the source plane and the top of the eMLC are coincident). A random number η is selected in the interval (0, 1], and if $\eta < (S/N_{\mathrm{split}})$ then a photon of weight N_{split} is generated according to the joint angular/spectral distribution and simulated beginning from the bottom surface of the MLC. In these simulations, N_{split} was set at 10, thus utilizing a Russian roulette-style variance reduction technique. The assumption was made that the bremsstrahlung phase space was invariant across the field, and that at a given point the photon distribution was radially symmetric. The low-energy electrons produced in the leaves were also ignored. This greatly simplifies and accelerates both source model generation and reconstruction, and it is shown in section 3.1.3 that these assumptions allow for sufficient accuracy for treatment planning.

2.1.4. Absolute dose calibration.

In general, Monte Carlo results are given in dose per incident particle. To convert to absolute dose, the dose distribution from a 15×15 cm^2 field is calculated (for each separate energy) and the central axis maximum taken to be a calibration factor, $D_{\mathrm{ref}}^{\mathrm{ref}}$ (here, subscripts refer to fields and superscripts refer to measurement points). This value is given in cGy/particle. Then, an arbitrary point A in the reference field may be converted to absolute dose per monitor unit D, given in cGy MU^{-1} by

$$D = \frac{D_{\mathrm{ref}}^{A}}{D_{\mathrm{ref}}^{\mathrm{ref}}}. \tag{4}$$

Because some particles are ignored for various reasons during conversion from phase space to source parameter (particles going backwards, positrons, field size limits, etc), this simple calculation is only valid for a single source parameter file. To be used in any field (in particular, here, the 25×25 cm^2 field), equation (4) may be expanded as

$$\frac{D_{25 \times 25}^{A}}{D_{\mathrm{ref}}^{\mathrm{ref}}} = \frac{D_{25 \times 25}^{A}}{D_{25 \times 25}^{\mathrm{ref}}} \times \frac{D_{25 \times 25}^{\mathrm{ref}}}{D_{\mathrm{ref}}^{\mathrm{ref}}}. \tag{5}$$

The term $D_{25 \times 25}^{\mathrm{ref}}$ can be calculated directly by simulating a 25×25 cm^2 field. The second factor, $D_{25 \times 25}^{\mathrm{ref}}/D_{\mathrm{ref}}^{\mathrm{ref}}$ cannot be taken from source parameter based Monte Carlo calculations, for reasons described above. i.e. some particles are not included during source parameter generation. However, this energy-dependent parameter may be taken from Monte Carlo simulations based on complete phase-space data or from measured applicator factors, defined as the ratio of absolute doses at the central axis maxima.

2.2. Optimization

The optimization method used was developed by Jiang (1998) and the salient features are described here. The system utilizes a steepest descent search algorithm, with a quadratic objective function augmented by dose–volume constraints. As usual, deviations from the prescribed dose p_0 contribute to the objective function in the following form

$$F_{\mathrm{target}} = \sum_{i \in T} (d_i - p_0)^2 \tag{6}$$

with T denoting points in the target. The soft dose–volume constraints are given by Zangwill's penalty function (Buchanan and Turner 1992). In particular,

$$F_{\mathrm{target}}^{\mathrm{penalty}} = w_{\mathrm{target}}^{\mathrm{low}} \sum_{i \in T} \xi_i^{\mathrm{low}} (d_i - p_1)^2 + w_{\mathrm{target}}^{\mathrm{high}} \sum_{i \in T} \xi_i^{\mathrm{high}} (d_i - p_2)^2 \tag{7}$$
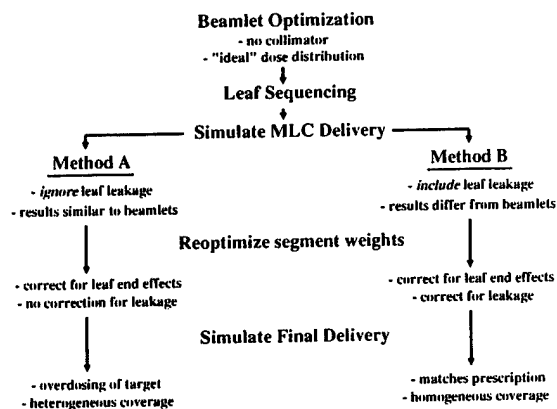
Beamlet Optimization
- no collimator
- "ideal" dose distribution

↓

Leaf Sequencing

↓

Simulate MLC Delivery

Method A
- *ignore leaf leakage*
- results similar to beamlets

Method B
- *include leaf leakage*
- results differ from beamlets

Reoptimize segment weights

- correct for leaf end effects
- no correction for leakage

- correct for leaf end effects
- correct for leakage

Simulate Final Delivery

- overdosing of target
- heterogeneous coverage

- matches prescription
- homogeneous coverage

Figure 2. A schematic summary of the overall treatment plan. Each stage is discussed in detail in the text. 'Method A' utilizes a simplified leaf model and is shown to result in an inferior plan. 'Method B' utilizes either explicit particle transport in the leaves or a bremsstrahlung approximation, and results in a delivered doses that match well with prescriptions.
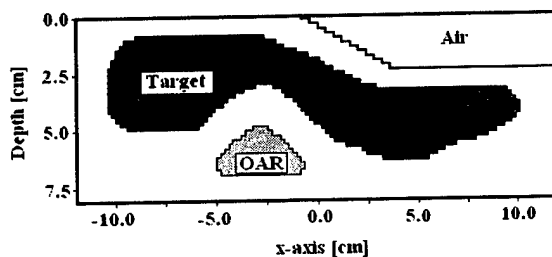

Figure 3. Schematic diagram of the test phantom. The target structure and organ at risk (OAR) are shaded and labelled accordingly. An extended air gap exists in the positive x region with the accelerator isocentre located at the origin of the diagram. The phantom material is ICRU tissue. The phantom extends 10 cm above and below the plane of the page.

where d_i is the dose at a point i, p_1 and p_2 are the upper and lower limits on target dose, w are the weights for the constraints and ξ_i is defined as 1 if the point i is too high/low *and* the volume constraint (number of points already in violation) has been reached. Similarly, critical structures are protected by adding upper-limit penalties in a dose–volume fashion. The overall objective function is then defined as

$$F_{obj} = F_{target} + r(F_{target}^{penalty} + F_{critical}^{penalty})$$ (8)

where r rises with each Zangwill iteration. Further details on this method of optimization may be obtained from Jiang (1998).

3. Results and discussion

The general outline of the treatment planning procedure is given in figure 2. On occasion, the text will refer to 'method A' or 'method B'. These will correspond with the appropriate branch of the flowchart in figure 2.
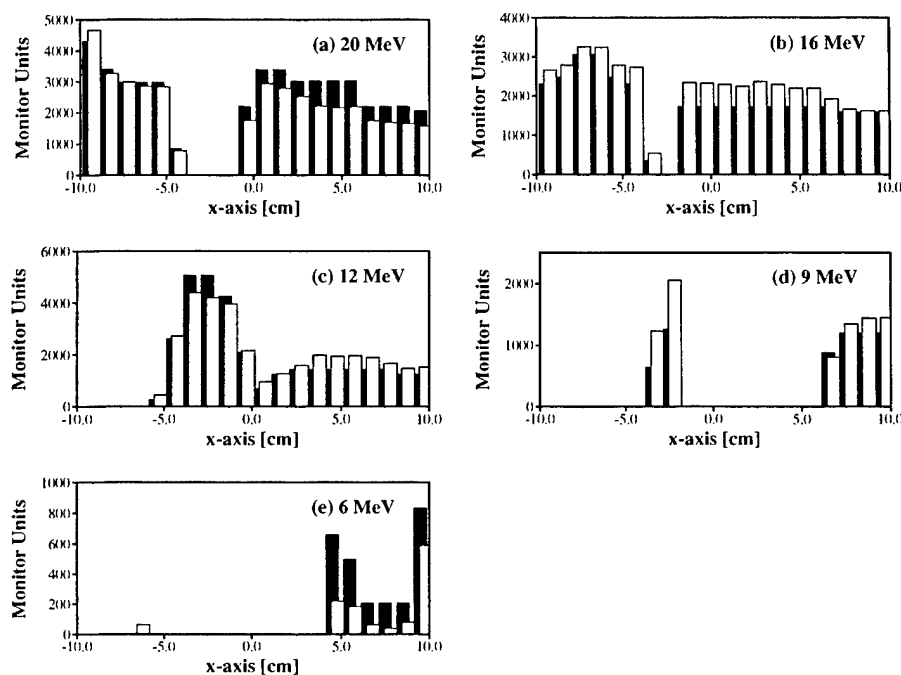
Figure 4. Intensity maps generated for the homogeneous phantom by optimization of electron beamlets: (a) 20 MeV, (b) 16 MeV, (c) 12 MeV, (d) 9 MeV, (e) 6 MeV. Shown are □, after initial beamlet optimization and ■, after final segment optimization. Note that the intensities shown for beamlets are prior to rebinning.

3.1. Homogeneous phantom

3.1.1. Geometry and beamlets.
The first phantom geometry to be considered was a two-dimensional homogeneous phantom with a sloped surface, shown schematically in figure 3. The two-dimensional system was chosen so that beamlet weights and dose distributions could be more easily assessed. The target was chosen to be concave with a critical structure placed within the concavity. A small region around the target was chosen to represent the normal tissue dose. The lateral extent of the target was approximately 20 cm. In the third dimension, i.e. out of the page, as shown, the target region was 4 cm wide and was surrounded by homogeneous ICRU tissue to a total width of 20 cm. The isocentre was placed at the surface of the phantom, centred on the x-axis.

An array consisting of 20 beamlets, each with an area of $1 \times 7 \text{ cm}^2$, was delivered into the phantom at each of the five available energies, covering the area from $x = -10.0$ to 10.0 cm. The 7 cm beamlet size along the y-axis was chosen to be sufficiently large such that the central target voxels were covered by a uniform field.

The beamlet weights were optimized to provide the intensity map shown in figure 4. The general trend is as expected based on energies and depths. That is, the higher (20 and 16 MeV) beams are restricted to the deeper target regions, while the lower energies are used in regions where sparing of the critical structure is necessary. The resulting cumulative dose–volume histogram (DVH) is shown in figure 5. Note that the target is well covered at the level of dose prescription and the coverage is uniform to within the statistics given in table 1.
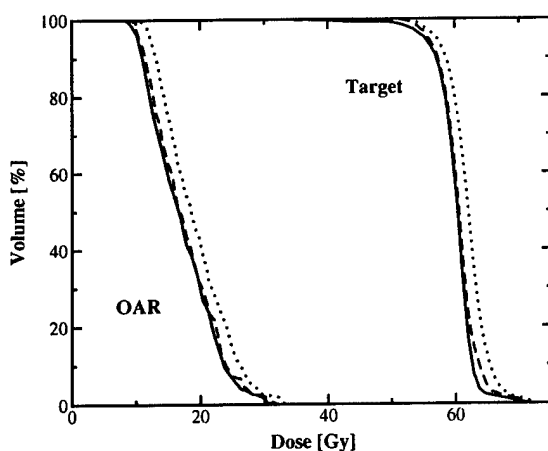
Figure 5. Cumulative DVHs for the homogeneous phantom based on a leaf sequence derived from the beamlet optimization (before the second optimization). Shown are DVHs for target and critical structures. The results are for beamlet simulation (———), full simulation of leaves (·····), and with leaf end scatter but no leakage (- - - -). The full simulation is what would actually be delivered, including a significant overdosing because of bremsstrahlung from the leaves. This overdose is not predicted by the other simulations.

Table 1. Dose constraints used during optimization of plans. For the target, a prescription dose of 60 Gy was assigned for the homogeneous phantom and 50 Gy for the breast phantom. In both cases, the average dose met this prescription to within 1%. Dose volume constraints are given as maximum or minimum dose allowed for a given volume (Prescr.). When this constraint is violated, penalties are assessed according to equation (7).

| | | | | % Volume exceeding dose limit | | |
	Structure	Dose (Gy)	Relative weight	Prescr.	Initial opt.	Final opt.
Homogeneous phantom	Target	>61.0	100.0	1.0	35.7	35.1
		<59.0	100.0	0.0	25.9	27.6
	OAR	>30.0	50.0	5.0	1.5	2.4
		>20.0	50.0	25.0	29.7	32.1
		>5.0	50.0	75.0	100.0	100.0
Breast phantom	Target	>50.5	100.0	0.0	38.0	34.6
		<49.5	100.0	0.0	38.7	33.7
	Rt Lung	>1.0	25.0	50.0	61.8	100.0
		>3.3	25.0	30.0	43.6	55.4
		>9.2	25.0	20.0	19.1	22.7

3.1.2. Simulation of the leaf sequence. This intensity profile was converted to a step-and-shoot leaf sequence (for a single, wide leaf) via the close-in method (Bortfeld *et al* 1994). The leaf sequencing method was chosen arbitrarily, but it is expected that the results should be general to any given leaf sequencing system (see section 3.2, for example). The delivery of this leaf sequence was then simulated with the leaves accounted for using two different methods: (A) no particles transported in leaves and consequently, no bremsstrahlung production in the leaves, and (B) explicit transport of electrons down to 2.0 MeV (ECUT) and photons to
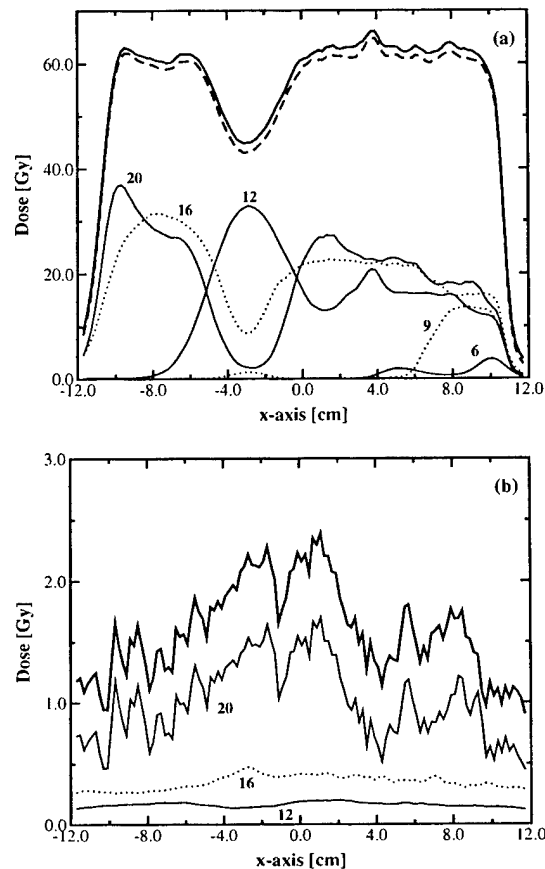
Figure 6. Dose profile from the simulated delivery of a plan based on beamlet optimization results (before the second optimization). (*a*) Dose profile taken at a depth of 4.0 cm below isocentre. Thin curves (full and dotted for clarity) represent individual energies while the thick curves indicate total dose, —— with. - - - - without bremsstrahlung. (*b*) A difference plot representing the bremsstrahlung contribution for each energy and the total plan (thick curve). For clarity, 9 and 6 MeV have been omitted. These low energies result in considerably less bremsstrahlung leakage than the energies displayed.

10 keV (PCUT). In all cases, complete simulation of all particles down to the global cut-offs was performed in an area within 5 mm of the leaf boundaries.

The DVHs for these deliveries are shown in figure 5. There are significant differences in the DVHs based on the type of leaf simulation. When bremsstrahlung is ignored (method A), the delivered DVH closely matches the DVH generated during beamlet delivery, with small differences caused by the finite thickness of the leaves and scatter off the leaf ends. The similarity between these two curves suggests that the beamlets and leaf delivery are implemented properly both in relative and absolute dose calculation. The difference between the beamlet optimization result and simulation via method A is due to the combined effects of leaf end scatter and rebinning the weights into 10 intensity levels. These effects are observed to have only a small impact on the resulting DVHs for this case.
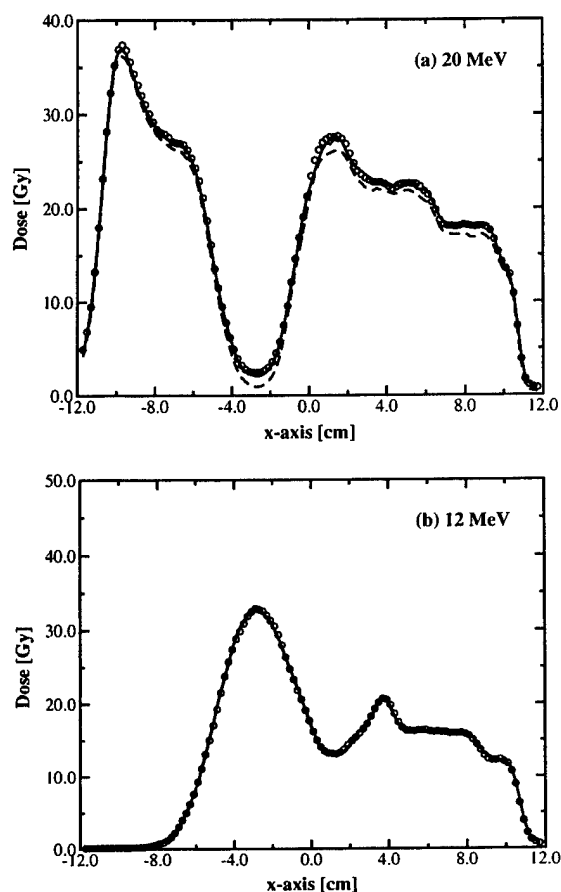
Figure 7. Dose profiles taken at a depth of 4.0 cm below isocentre for (*a*) 20 MeV and (*b*) 12 MeV. Shown are explicit simulation (——), no bremsstrahlung production in leaves (- - - -), and approximated leakage (O). Note the magnitude of the bremsstrahlung dose (the difference between no transport and explicit simulation) at 20 MeV and the agreement between the approximate and explicit simulation.

This, however, represents only the ideal case and one that cannot be delivered with a real collimator system. When the actual eMLC delivery is simulated, including bremsstrahlung production in the leaves (method B), it is apparent that a significant increase in dose occurs in both the critical structure and target. This suggests that bremsstrahlung leakage is an essential element in the dose calculation.

Figure 6(*a*) shows the contribution of each energy to the total dose at a depth of 4.0 cm. As expected, the dose distribution of each energy roughly follows the intensity maps of figure 4. The difference in absolute dose between the complete plan delivered with and without bremsstrahlung leakage, taken at the same depth, is shown in figure 6(*b*). What is immediately apparent is that, as expected, the primary contributor to bremsstrahlung background is the 20 MeV field. Profiles at different depths show similar results. It is also observed that the
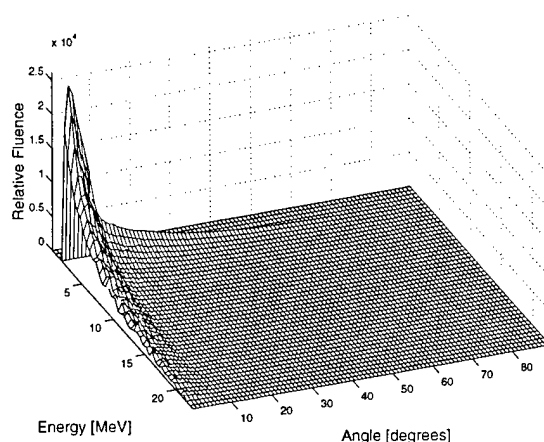
Figure 8. The joint angular/spectral distribution for bremsstrahlung photons generated in a 1.5 cm tungsten slab irradiated by the 20 MeV field of a Varian Clinac 2100C. The distribution is given as an average over the entire field. The z-axis is presented in arbitrary units of planar fluence. Integrated over all angles. the most probable energy for this distribution is 2.25 MeV with a mean energy of 5.06 MeV.

effect is not uniform, and is thus not likely to be corrected by a global change in monitor units delivered.

This leaf effect can be studied in more detail by examining dose profiles for individual energies, as shown for 20 and 12 MeV in figure 7. Examining the 20 MeV profile in figure 7(a), taken at a depth of 4.0 cm, it can be seen that the full leaf simulation gives a slightly higher dose across the field, especially in the region corresponding to the critical structure. In this region, adequate coverage was achieved by the use of the 12 MeV field because the target stopped at a shallower depth. Because the 20 MeV would penetrate into the critical structure, it was blocked in this region. However, while primary electrons are blocked, bremsstrahlung is generated by the electron interactions in the leaves.

Thus, there exists here a situation where the open field (12 MeV) delivers dose as predicted by the beamlet simulation, but leakage dose from closed fields (20 MeV) is not accounted for during beamlet optimization. In this case, an appropriate correction can be found by inspection: the intensity of the portions of the 12 MeV overlaying the critical structure should be reduced in such a way as to (at least partially) offset the dose being delivered by the bremsstrahlung from the 20 MeV field. Of course, this only offers an approximate correction to one region which may not be the optimal correction even for this limited problem, and does not correct for leaf end scatter. As noted, leaf end scatter plays a small role in this case, but situations may arise in which it has a larger impact than bremsstrahlung production, especially if low-energy fields are delivered with higher intensities. A more robust and automated solution is necessary for use in treatment planning. This can be achieved by the optimization of segment weights.

3.1.3. Bremsstrahlung approximation. These results clearly indicate that the effect of bremsstrahlung leakage must be included during treatment planning. However, transporting particles through the leaves becomes prohibitively slow when multisegment, multienergy plans are considered. A method to approximate the leakage was then developed to circumvent this problem.

Table 2. A comparison of the three different methods of leaf simulation. All values are taken at a depth of 2.5 cm. The open portion of the field extended from the central axis towards the $+x$ direction. The 'dose out of field' was computed as the average of the dose from -10.0 cm to -3.5 cm. Relative speeds are presented normalized to the full, or explicit, simulation. See section 2.1.3 for details on each simulation method. The same number of initial particles were simulated in each case. The statistical uncertainty was approximately 0.5% at 1σ.

Field	Leaf simulation method	Relative speed	Max. dose in field		Dose out of field	
			(Gy)	Rel. error	(Gy)	Rel. error
20 MeV	Explicit	1.0	10.05	—	0.16	—
5×7 cm^2	No trans.	5.1	9.98	<1%	0.01	−92.4%
	Approx.	4.3	10.01	<1%	0.16	<1%
20 MeV	Explicit	1.0	8.27	—	0.15	—
1×7 cm^2	No trans.	13.3	8.14	−1.54%	0.01	−96.3%
	Approx.	8.2	8.50	+1.03%	0.16	<1%

Just as a source model is used to generate electrons and photons from the treatment head, a bremsstrahlung source model was used to re-create photons at the lower surface of the eMLC, as described in section 2.1.3. The joint angular/spectral distribution for a 20 MeV field as generated by EGS4/BEAM simulation is plotted in figure 8. As expected, the photons are primarily forward directed with a significant low-energy portion. The approximation was tested on simple static fields and found to reproduce full simulation results to within 2%. The improvement in speed and specific dose values can be found in table 2. In particular, for the 1 cm field where only about 3% of the eMLC is open (as is the case in many plan segments), the simulation could be accelerated by approximately a factor of 8.

A second set of simulations was executed for these leaf settings, again with full leaf simulation. The BLCMIN parameter of the PRESTA algorithm was set to 1.5 to maintain smaller step sizes than are necessary for accurate transport (Bielajew and Rogers 1987). It has been reported that this may lead to a small but significant change in the bremsstrahlung yield in thick targets (Faddegon *et al* 1990, 1991). However, no significant changes were observed in the bremsstrahlung dose distributions, and so the default PRESTA values were retained (for speed) in all subsequent simulations. However, it is noted that the true bremsstrahlung spectrum, yield and angular distributions may indeed differ significantly from the approximate source used here, though the effect on the resulting dose is trivial compared with the primary electron dose.

In section 3.1.2, it was proposed that optimizing segment weights may correct for bremsstrahlung leakage. This will be most effective if the bremsstrahlung angular spread is sufficiently narrow such that open regions received only trivial photon dose during the delivery of that segment. Indeed, this assumption is validated by the results shown in table 2. For the 1 cm wide field, the difference between maximum doses with explicit leakage and no leakage is approximately 1.6% on a statistical uncertainty of 1.0%. The overdose caused by the approximation in the open field region is similarly within 2%. This error is due to the approximation that the bremsstrahlung angular distribution is the same at all points, rather than tilted away from the central axis (as the incident electrons are). However, especially as this effect decreases with increasing field size, it was considered an acceptable level of error.

The method presented is one possible method to simulate the effect of the leaves in an acceptable time frame, and was used for the CT phantom in section 3.2. For the homogeneous phantom currently under discussion, DVHs and isodose lines for simulations performed using
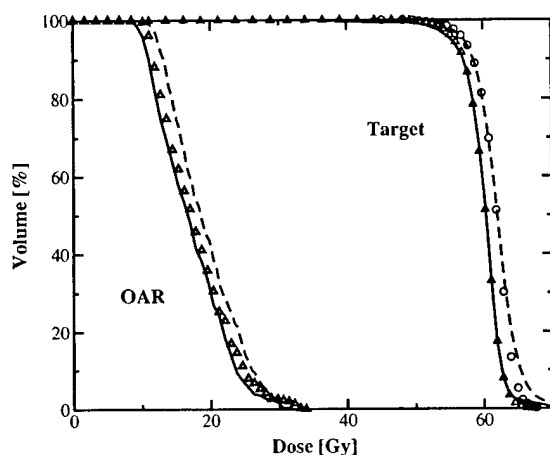
Figure 9. Cumulative DVHs for the homogeneous phantom for target and critical structure, after beamlet optimization (——), simulated delivery of this plan with leaves in place. i.e. without second optimization (- - - -), and simulated delivery with leaves after segment optimization. i.e. final plan (△). Note that the original beamlet optimization and the final plan are nearly indistinguishable in target coverage. Also shown is the delivered target DVH for a plan in which a second optimization occurred, but in which segments only included leaf scatter, and not bremsstrahlung (O).

this approximation and explicit full leaf simulation were found to be indistinguishable. Thus, unless otherwise specified, figures and discussion regarding explicit simulation of leaves are equally applicable to the approximate bremsstrahlung approach.

3.1.4. Optimization of segment weights. During the simulated delivery of the leaf sequence, the dose distribution from each segment was stored separately. A segment was defined as the beam delivered by a field defined by a set of leaf positions, that is, a single static field in a step-and-shoot sequence. Treating each of these segments as if they were beamlets, the weights, or monitor units delivered per segment, were re-optimized with the same parameters as before. The initial conditions for the optimization were taken from the original monitor unit settings, i.e. those derived from the first beamlet optimization. The results of this second optimization are shown in table 1.

It is crucial to recall that this second optimization is based on a realistic geometry and includes such details as leaf end transmission and bremsstrahlung leakage. In contrast, the results of the first optimization are based on idealized beamlets, i.e. with no real collimator geometry involved. This first optimization gives the best dose distribution with a given optimization (given a perfectly absorbing and infinitely thin collimator), while the second optimization is the actual delivered dose. What is observed is that if the non-idealities caused by the eMLC are included in the second stage optimization (i.e. the segment optimization), the final result does not deviate far from the ideal case (i.e. the beamlet optimization). The target dose and coverage are very similar, with a slight increase in dose to critical structures. Note that of course the bremsstrahlung dose cannot be completely negated, and that there is a small increase in dose to normal tissues as a result, but this occurs deeper than the target and critical structure and thus represents doses of less than 2% of the prescription dose.

These results are further detailed in figure 9, where the DVHs are shown after various stages of planning. Idealized beamlets are optimized to give a dose distribution that agrees very well
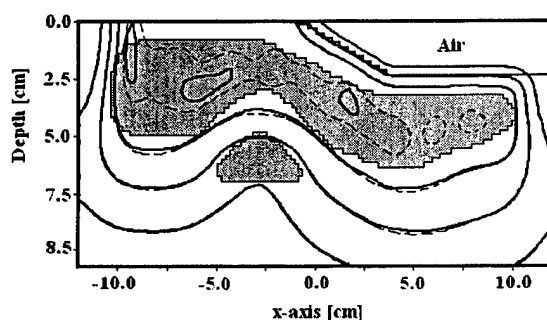
Figure 10. Isodose lines for the homogeneous phantom. Shown are the simulated deliveries of plans generated accounting for leaf effects (———) and plans that ignored the effect of the leaves (- - - -). The structures are labelled in figure 3. Lines represent absolute doses: starting closest to the target and moving outwards, 62.5, 50, 30, 10 Gy. Recall that the prescription dose was 60 Gy. Target doses in both cases satisfied the minimum prescription dose requirements, but there is significant overdosing of the target in the plan that did not account for leaf effects.

with the prescription on table 1, shown as full curve in the figure. However, actually delivering this plan adds the effect of the collimator leakage and scatter. The resulting DVH is shown as a broken curve, and is right shifted and also has a change in the slope, suggesting much poorer target coverage than was predicted by the idealized plan. However, once segment weights are re-optimized, the DVHs, shown as symbols, indicate that target coverage is very similar to that of the ideal beamlets, despite the non-idealities of the real collimator. The dose to critical structures rises slightly with the addition of the leaves, due to the leakage, but the final optimization does reduce this effect somewhat. The resulting intensity maps are shown in figure 4.

It is noted that this optimization is a somewhat smaller problem than the initial optimization. In particular, whereas the initial optimization was in 100 dimensions (20 beamlets × 5 energies), this second optimization has a dimensionality equal to the total number of segments in all ports: in this case, 33. Additionally, the initial values of the segment weights are much closer to the optimal solution than the initial beamlet weights, which were set to zero.

3.1.5. Final dose distributions. As implemented, the optimization procedure involves storage of complete information about dose in structures (target, OAR) but only stores dose for a limited set of healthy tissue voxels. Thus, while the DVHs generated in the second optimization are complete, plotting isodose lines and a full accounting of normal tissue dose requires a final dose calculation based upon the entire plan. While it is possible that this step could be avoided in a clinical implementation (given sufficient computer resources), it was also a necessary step for this study to fully quantify the error introduced by ignoring the leaf transport.

Figure 9 shows the DVHs for the final deliveries planned based on full leaf transport simulations and also a plan generated with only leaf scatter accounted for. Both plans were based on an intensity map generated by the same ideal beamlets. This initial optimization result gave the leaf positions for the deliveries. At this point, both simulations are identical. Then, the delivery of the leaf sequence was simulated with leaf leakage included in one case and ignored in the other. In the case where bremsstrahlung from the leaves was ignored, the finite thickness of the leaves and end scatter and transmission was still included. The segment weights for these two simulations were then re-optimized, such that a final set of leaf positions
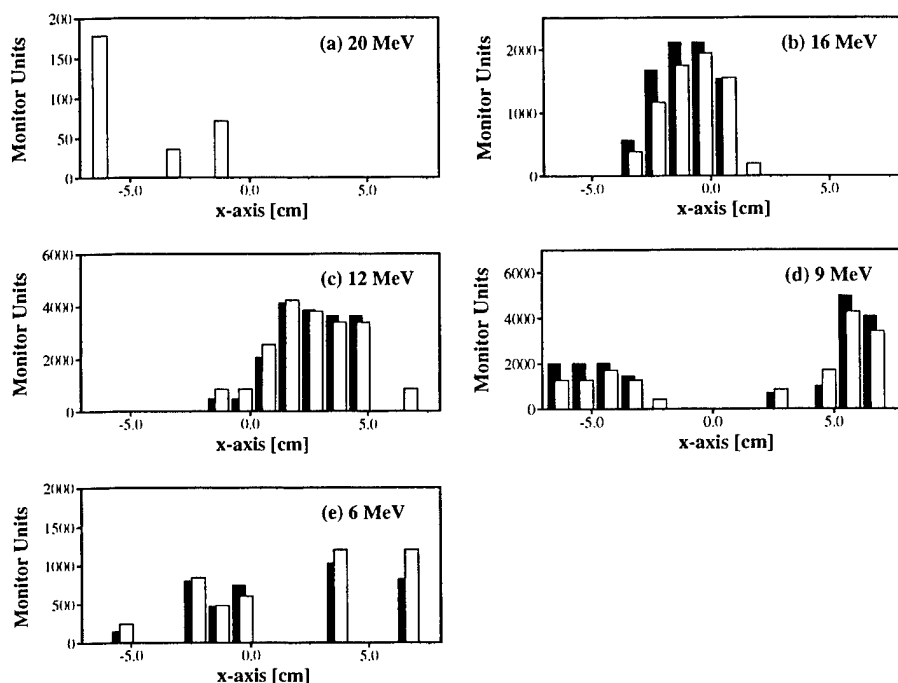
Figure 11. Intensity maps for the AP field of the 2D breast plan. generated by optimization of electron beamlets, for the AP directed port: (*a*) 20 MeV. (*b*) 16 MeV. (*c*) 12 MeV. (*d*) 9 MeV. (*e*) 6 MeV. Shown are □. after beamlet optimization and ■. after segment optimization.

(based on the first optimization) and monitor units (based on the second optimization) were obtained. These were then simulated with complete simulation of the collimator system, to observe the dose distributions from actual deliveries based on these planning procedures.

As expected, figure 9 shows that the delivery that was planned without leaf leakage resulted in an overdose to the target and critical structures. This is expected to be true for any situation in which the leaf transport and leakage is not properly included in the simulation, not just simulations in which all transport is ignored. Note that the DVHs for the plan generated with the bremsstrahlung approximation are virtually indistinguishable from the full simulation DVHs, and are thus not shown.

Isodose plots are shown in figure 10 for the plans generated with the leaf effect included in the optimization and for plans that did not take this leaf effect into account. What is apparent is that failing to include leaf effects in planning leads to an overdosing, shown by the 62.5 Gy isodose line.

## 3.2. Two-dimensional breast CT phantom

As a demonstration of this method in a more realistic scenario, a plan was generated for irradiation of an intact breast. For this proof-of-principle study, the breast was taken as a single CT slice. Extension to 3D cases requires further study on the effect of leaf sequences on MERT planning, and will be addressed in future research. Details of the planning parameters and results can be seen in table 1.
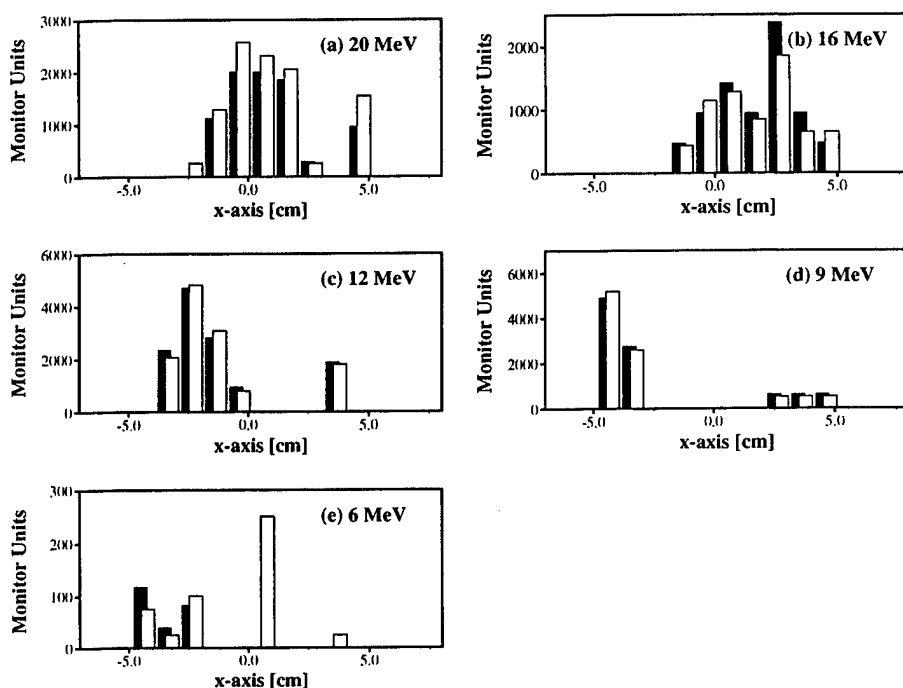
Figure 12. Intensity maps for the RL field of the 2D breast plan, generated by optimization of electron beamlets, for the right lateral port: (*a*) 20 MeV, (*b*) 16 MeV, (*c*) 12 MeV, (*d*) 9 MeV, (*e*) 6 MeV. Shown are □, after beamlet optimization and ■, after segment optimization.

For this plan, two ports with different gantry angles and isocentres were employed, with five energies delivered through each port. One port is directed in the anterior–posterior (AP) direction while the second port was directed from the right lateral (RL) direction. The planning proceeded using the method developed in the discussion of the homogeneous phantom (i.e. via method B). Beamlets were delivered and optimized, a leaf sequence was derived for the eMLC, delivery was simulated using the bremsstrahlung approximation and the segment weights were re-optimized. While the homogeneous leaf sequence was generated using the close-in method, this leaf sequence was generated using the intensity solid paradigm method of Siochi (1999), as a demonstration of the generality of the planning procedure. No other modifications to the planning scheme described above were necessary for simulation of this multiport/multi-isocentre plan.

The intensity maps for the AP fields are shown in figure 11 and the RL fields are shown in figure 12. Unlike the single-port homogeneous plan discussed earlier, the intensity maps are less intuitive and are, in a qualitative sense, less smoothly varying than the homogeneous phantom discussed earlier. The addition of a second gantry angle and homogeneous material makes this optimization more similar to photon IMRT in that intensity maps can only be roughly estimated by inspecting the geometry. However, the general trend of reducing 20 MeV field intensities and compensating for this with increased intensity at the lower energies is maintained. Further research will examine the effect of smoothing these profiles, as has been suggested for photon IMRT.
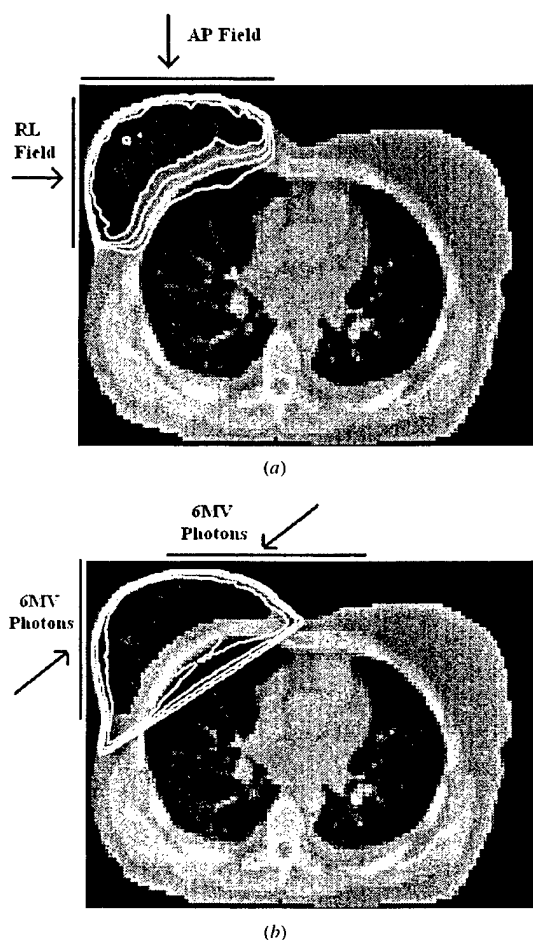
Figure 13. Isodose lines for the 2D breast plan. (*a*) MERT final delivery after both beamlet and segment optimization are complete. (*b*) A pair of tangential photon beams. Starting closest to the target and moving outwards, 48, 40, 30, 20 Gy.

(This figure is in colour only in the electronic version, see www.iop.org)

The resulting dose distribution for the MERT plan is shown in figure 13(*a*). A second set of isodose lines are plotted in figure 13(*b*) for a pair of 6 MV tangential photon beams directed onto the breast as per standard protocols. The lateral photon field utilized a 45° wedge and the relative weights of the two fields was optimized. The corresponding DVHs are shown in figure 14. The low lung dose in the MERT plan is a combination of two factors: the two-port set-up and the use of lower-energy beams for the thinner portions of the breast. Note that achieving a homogeneous dose with two electron ports necessitates intensity modulation. Note, also, that the DVH volumes are presented as percentages of this slice only, and not as a percentage of the entire lung.

This represents a case where conventional treatments are often non-optimal, as tangential photon beams often result in heterogeneous dose, scatter dose to the contralateral breast and
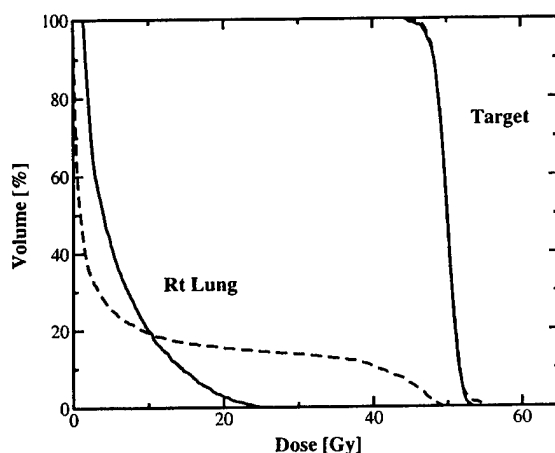
Figure 14. Cumulative DVHs for the 2D breast plan. ———, simulation of final delivery plan with leaves in place and - - - -, tangential 6 MV photon beams. Note that volumes actually represent area in this slice, as the plan was conducted in two dimensions.

the necessity of a large margin to compensate for breathing motion. In this case, the breathing motion was assumed to be primarily expansion in the direction normal to the tangential beams. While this two-port MERT plan is also affected by breathing motion, the effect is somewhat lessened as the beams still retain an acute angle of incidence relative to the breathing motion. In contrast, the photon plan includes a much larger region of the breast in the high-dose region, as a large margin must be included because breathing motion is in a direction largely orthogonal to the beam angles. A complete study of the impact of breathing motion on the two treatment modalities will be of significant interest, but is beyond the scope of this work. Regardless of the margin, the curvature of the chest wall and the lateral extent of the clinical target region dictate that some amount of normal tissue and lung will be included in the high-dose region.

Note that this case has been presented as a proof-of-principle for both the potential role of MERT in a clinical scenario and of the efficacy of this planning scheme. Examining the utility of MERT at different anatomical sites and a full comparison with other treatment modalities is beyond the scope of this paper.

4. Conclusions

This study has demonstrated the feasibility of MERT with a scattering foil linear accelerator. Two primary objections voiced against MERT have been that the in-air scatter is too great to have an acceptable resolution and that this scatter will hinder the optimization process. The scattering problem has been minimized by the design of the electron MLC. There is certainly an appreciable amount of air scatter, especially at the lower energies; however, it has been shown that this does not significantly affect dose distributions in the model targets. Furthermore, optimization of electron beamlets will be inherently inaccurate if poor electron transport algorithms are used to account for in-air transport. This problem has been overcome with the use of Monte Carlo transport algorithms. The beamlet dose profiles may have wide penumbras or other non-ideal characteristics, but as long as this information is incorporated into optimization, the final result will be physically correct.

While this study has employed a specific model of an electron MLC and a specific Monte Carlo dose calculation system and optimization software, it should be noted that these results can be generalized to other situations. That is, the effect of any real collimator that perturbs the delivered beam away from the idealized beamlets can be at least partially accounted for by this two-step optimization procedure. Also, any dose calculation system and optimization software may be used, provided that transport in non-patient regions such as the air gap and eMLC can be performed accurately.

With rapidly increasing Monte Carlo calculation speeds and improvements in computer hardware, it is likely that calculating MERT plans in the manner described will soon be possible on a time scale easily comparable to advanced analytical photon planning algorithms. Thus it is important to pursue additional research in MERT planning, focusing on development of three-dimensional planning techniques. Currently, three-dimensional plans may be generated using the methods presented. However, it is anticipated that the method used to organize individual leaves into a synchronous leaf sequence will have some bearing on the ability to compensate for leakage. Further research will also examine specific treatment planning considerations, such as changing the number of energy and intensity levels, as well as adding additional gantry angles or isocentres, and combining photons and electrons in a single plan.

Acknowledgments

References

Åsell M, Hyödynmaa S, Gustafsson A and Brahme A 1997 Optimization of 3D conformal electron beam therapy in inhomogeneous media by concomitant fluence and energy modulation *Phys. Med. Biol.* **42** 2083–100

Åsell M, Hyödynmaa S, Söderstroöm S and Brahme A 1999 Optimal electron and combined electron and photon therapy in the phase space of complication-free cure *Phys. Med. Biol.* **44** 235–52

Bielajew A F 1994 Monte Carlo modelling in external-beam radiotherapy—why leave it to chance? *Proc. 11th Int. Conf. on the Use of Computers in Radiation Therapy* ed A R Hounsell, J M Wilkinson and P C Williams (Manchester: North Western Medical Physics Department, Christie Hospital NHS Trust) pp 2–5

Bielajew A F and Rogers D W O 1987 PRESTA—the parameter reduced electron step algorithm for electron Monte Carlo transport *Nucl. Instrum. Methods* B **18** 165–81

Bielajew A F, Rogers D W O, Cygler J and Battista J J 1987 A Comparison of electron pencil beam and Monte Carlo calculational methods *The Use of Computers in Radiation Therapy* ed I A D Bruinvis (Amsterdam: Elsevier) pp 65–8

Bortfeld T R, Kahler D L, Waldron T J and Boyer A L 1994 X-ray field compensation with multileaf collimators *Int. J. Radiat. Oncol. Biol. Phys.* **28** 723–30

Boyer A L and Mok E C 1985 A photon dose distribution model employing convolution calculations *Med. Phys.* **12** 169–77

Buchanan J L and Turner P R 1992 *Numerical Methods and Analysis* (New York: McGraw-Hill)

Chen Y, Boyer A L and Ma C-M 2000 Calculation of x-ray transmission through a multileaf collimator *Med. Phys.* **27** 1717–26

Cygler J, Battista J J, Scrimger J W, Mah E and Antolak J 1987 Electron dose distributions in experimental phantoms: a comparison with 2D pencil beam calculations *Phys. Med. Biol.* **32** 1073–83

Ebert M A and Hoban P W 1997 Possibilities for tailoring dose distributions through the manipulation of electron beam characteristics *Phys. Med. Biol.* **42** 2065–81

Faddegon B A, Ross C K and Rogers D W O 1990 Forward directed bremsstrahlung of 10–30 MeV electrons incident on thick targets of Al and Pb *Med. Phys.* **17** 773–85

Faddegon B A, Ross C K and Rogers D W O 1991 Angular distribution of bremsstrahlung from 15 MeV electrons incident on thick targets of Be, Al and Pb *Med. Phys.* **18** 727–39

Hogstrom K R, Mills M D and Almond P R 1981 Electron beam dose calculations *Phys. Med. Biol.* **26** 445–59

Holmes T W 2001 A method to incorporate leakage and head scatter corrections into a tomotherapy inverse treatment planning algorithm *Phys. Med. Biol.* **46** 11–27

Hyödynmaa S, Gustafsson A and Brahme A 1996 Optimization of conformal electron beam therapy using energy- and fluence-modulated beams *Med. Phys.* **23** 659–66

Jansson T, Lindman H, Nygård K, Dahlgren C V, Montelius A, Öberg-Kreuger C, Asplund S and Bergh J 1998 Radiotherapy of breast cancer after breast-conserving surgery: an improved technique using mixed electron-photon beams with a multileaf collimator *Radiother. Oncol.* **46** 83–9

Jeraj R and Keall P 2000 The effect of statistical uncertainty on inverse treatment planning based on Monte Carlo dose calculation *Phys. Med. Biol.* **45** 3601–13

Jiang S B 1998 Development of a compensator based intensity modulated radiation therapy system *PhD Thesis* Medical College of Ohio, Toledo, OH

Jiang S B, Kapur A and Ma C-M 2000 Electron beam modelling and commissioning for Monte Carlo treatment planning *Med. Phys.* **27** 180–91

Kapur A 1999 Monte Carlo dose calculations for clinical electron and intensity modulated photon beams in radiotherapy *PhD Thesis* Stanford University, Stanford, CA

Kapur A, Ma C-M, Mok E C, Findley D O and Boyer A L 1998 Monte Carlo calculations of electron beam output factors for a medical linear accelerator *Phys. Med. Biol.* **43** 3479–94

Karlsson M G, Karlsson M K and Ma C-M 1999 Treatment head design for multileaf collimated high-energy electrons *Med. Phys.* **26** 2125–32

Karlsson M K, Karlsson M G and Zackrisson B 1998 Intensity modulation with electrons: calculations, measurements and clinical applications *Phys. Med. Biol.* **43** 1159–69

Kawrawkow I and Fippel M 2000 Investigation of variance reduction techniques for Monte Carlo photon dose calculation using XVMC *Phys. Med. Biol.* **45** 2163–83

Kawrakow I, Fippel M and Friedrich K 1996 3D electron dose calculation using a voxel based Monte Carlo algorithm *Med. Phys.* **23** 445–57

Keall P J, Siebers J V, Jeraj R and Mohan R 2000 The effect of dose calculation uncertainty on the evaluation of radiotherapy plans *Med. Phys.* **27** 478–84

Klein E E, Li Z and Low D A 1996 Feasibility study of multileaf collimated electrons with a scattering foil based accelerator *Radiother. Oncol.* **41** 189–96

Koch H W and Motz J W 1959 Bremsstrahlung cross-section formulas and related data *Rev. Mod. Phys.* **31** 920–55

Korevaar E W, Heijmen B J M, Woudstra E, Huizenga H and Brahme A 1999 Mixing intensity modulated electron and photon beams: combining a steep dose fall-off at depth with sharp and depth-independent penumbras and flat beam profiles *Phys. Med. Biol.* **44** 2171–81

Laub W Alber M, Birkner M and Nüsslin F 2000 Monte Carlo dose computation for IMRT optimization *Phys. Med. Biol.* **45** 1741–54

Lee M C, Jiang S B and Ma C-M 2000a Monte Carlo and experimental investigations of multileaf collimated electron beams for modulated electron radiotherapy *Med. Phys.* **27** 2708–18

Lee M C, Jiang S B, Yi B and Ma C-M 2000b Monte Carlo simulations of multileaf collimated electrons *Proc. 13th Int. Conf. on the Use of Computers in Radiation Therapy* ed W Schlegel and T Bortfeld (Heidelberg: Springer) pp 176–8

Lee M C, Kapur A, Jiang S B and Ma C-M 2000c Characterization of electron beams for modulated electron beam radiotherapy *CD-ROM Proc. of the World Congress on Medical Physics and Biomedical Engineering (23–28 July 2000)*

Li J S, Pawlicki T, Deng J, Jiang S B and Ma C-M 2000a Simulation of Beam Modifiers for Monte Carlo Treatment Planning *Proc. 13th Int. Conf. on the Use of Computers in Radiation Therapy* ed W Schlegel and T Bortfeld (Heidelberg: Springer) pp 437–9

Li J S, Pawlicki T, Deng J, Jiang S B, Mok E and Ma C-M 2000b Validation of a Monte Carlo dose calculation tool for radiotherapy treatment planning *Phys. Med. Biol.* **45** 2969–85

Lief E P, Larsson A and Humm J L 1996 Electron dose profile shaping by modulation of a scanning elementary beam *Med. Phys.* **23** 33–44

Ma C-M, Faddegon B A, Rogers D W O and Mackie T R 1997 Characterization of Monte Carlo calculated electron beams for radiotherapy *Med. Phys.* **24** 401–16

Ma C-M, Li J S, Pawlicki T, Jiang S B and Deng J 2000a MCDOSE—A Monte Carlo dose calculation tool for radiation therapy treatment planning *Proc. 13th Int. Conf. on the Use of Computers in Radiation Therapy* ed W Schlegel and T Bortfeld (Heidelberg: Springer) pp 123–5

Ma C-M, Mok E, Kapur A, Pawlicki T, Findley D, Brain S, Forster K and Boyer A L 1999 Clinical implementation of a Monte Carlo treatment planning system for radiotherapy *Med. Phys.* **26** 2133–43

Ma C-M, Pawlicki T, Lee M C, Jiang S B, Li J, Deng J, Yi B, Mok E, Luxton G and Boyer A L 2000b Energy- and intensity-modulated electron beam radiotherapy for breast cancer *Phys. Med. Biol.* **45** 2947–67

Ma C-M and Rogers D W O 1997 BEAMDP users manual *National Research Council of Canada Report* PIRS-0509c (Ottawa: NRC)

Mackie T R *et al* 1994 The OMEGA project: comparison among EGS4 electron beam simulations, 3D Fermi-Eyges calculations, and dose measurements *Proc. 11th Int. Conf. on the Use of Computers in Radiation Therapy* ed A R Hounsell, J M Wilkinson and P C Williams (Manchester: North Western Medical Physics Department, Christie Hospital NHS Trust) pp 152–3

Mah E, Antolak J, Scrimger J W and Pattista J J 1989 Experimental evaluation of a 2D and 3D pencil beam algorithm *Phys. Med. Biol.* **34** 1179–94

Mohan R 1997 Why Monte Carlo? *Proc. 12th Int. Conf. on the Use of Computers in Radiation Therapy* ed D D Leavitt and G Starkschall (Madison, WI: Medical Physics Publishing) pp 16–18

Mubata C D, Verhaegen F and Nahum A E 2000 Speeding up Monte Carlo simulation of electron cut-outs in treatment planning *Proc. 13th Int. Conf. on the Use of Computers in Radiation Therapy* ed W Schlegel and T Bortfeld (Heidelberg: Springer) pp 440–2

Nelson W R, Hirayama H and Rogers D W O 1985 The EGS4 code system *SLAC Report* 265 (Stanford, CA: Stanford Linear Accelerator Center)

Pawlicki T A, Jiang S B, Deng J, Li J S and Ma C-M 1999 Monte Carlo calculated beamlets for photon beam inverse planning *Med. Phys.* **26** 1064–5

Rogers D W O 1991 The role of Monte Carlo simulation of electron transport in radiation dosimetry *Int. J. Appl. Radiat. Isot.* **42** 965–74

Rogers D W O, Faddegon B A, Ding G X and Ma C-M 1995 BEAM: a Monte Carlo code to simulate radiotherapy treatment units *Med. Phys.* **22** 503–24

Seltzer S M and Berger M J 1985 Bremsstrahlung spectra from electron interactions with screened atomic nuclei and orbital electrons *Nucl. Instrum. Methods* B **12** 95–134

Siochi R A C 1999 Minimizing static intensity modulate delivery time using an intensity solid paradigm *Int. J. Radiat. Oncol. Biol. Phys.* **43** 671–80

van Santvoort J P C and Heijmen B J M 1996 Dynamic multileaf collimation without 'tongue-and-groove' underdosage effects *Phys. Med. Biol.* **41** 2091–105

Yu C X 1998 Design considerations for the sides of multileaf collimator leaves *Phys. Med. Biol.* **43** 1335–42

Zackrisson B and Karlsson M 1996 Matching of electron beams for conformal therapy of target volumes at moderate depths *Radiother. Oncol.* **39** 261–70

Energy and Intensity Modulated Electron Radiotheray: A Comparative Dosimetric Study of MERT and IMRT for Head & Neck Cancer

Y. Song, M. C. Lee, and A. L. Boyer

*Department of Radiation Oncology, Stanford University School of Medicine, Stanford, CA*

In this study, we investigated treating head and neck cancers using modulated electron radiation therapy (MERT) by comparing MERT plans with x-ray intensity-modulated radiation therapy (IMRT) in terms of target coverage and normal tissue sparing.

An experimental electron multi-leaf collimator was fabricated by modifying a conventional electron cone (Varian Medical Systems, Palo Alto, CA). Electron beams produced by a linac (Clinac 2100C, Varian Medical Systems) and collimated by this electron MLC were simulated using the EGS4/BEAM code. The simulations were based on the manufacturer's specifications of the beam production system and the electron cone design. The MERT plans with three coplanar beams (205^0, 235^0, and 255^0) and five nominal energies (6, 9, 12, 16, 20 MeV) were created using modified EGS4/MCDOSE code. The doses were checked against a commercially available Monte Carlo dose calculation engine (NXEGS, NumeriX LLC, New York, NY) and measurements. The IMRT plans with five coplanar beams were computed using a commercial treatment planning system (CORVUS, NOMOS Corp, Sewickley, Pennsylvania).

Our preliminary data indicated that MERT is able to provide similar target dose coverage compared with photon beam IMRT. However, MERT can significantly reduce the dose to critical structures. In the cases we studied, the maximum dose to the orbits, brainstem, optic chiasm, and spinal cord were reduced by 3.0, 16.2, 11.5, and 19.6 Gy, respectively, for a 50Gy target dose, suggesting a distinct normal tissue sparing advantage for MERT.
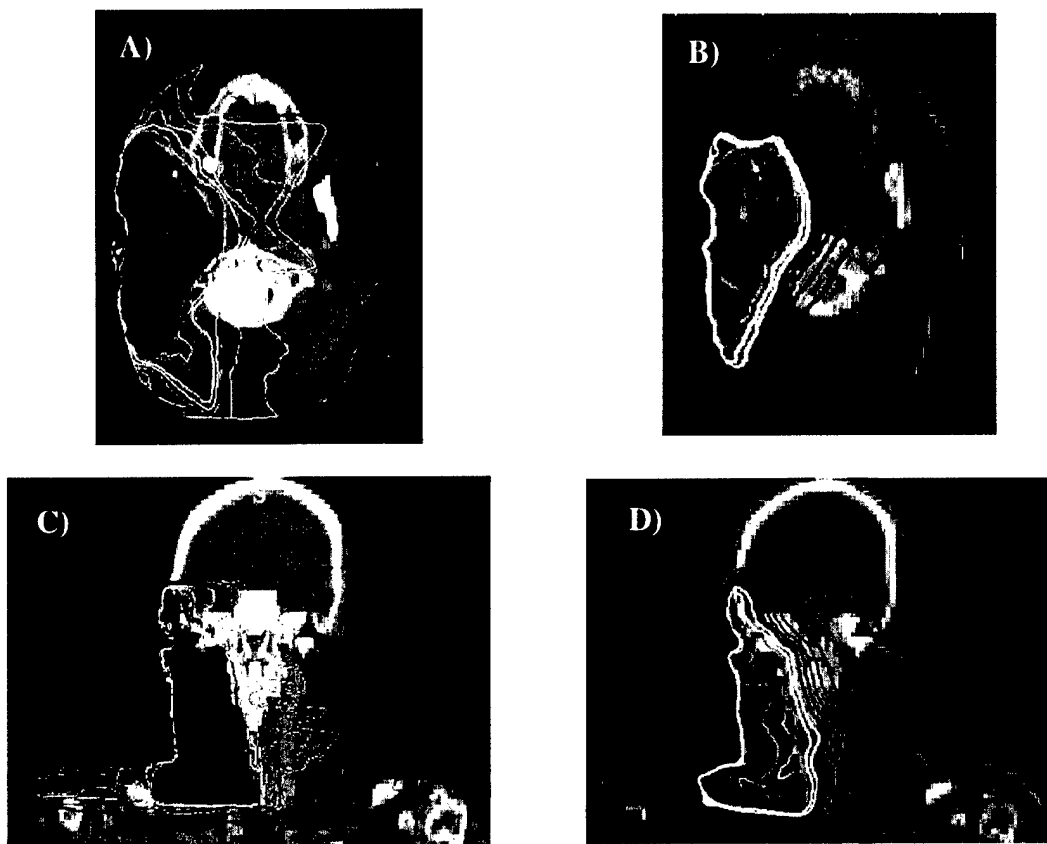
Figure 1. Comparison of dose distributions between the x-ray IMRT plan (**A, C**) and the MERT plan (**B, D**). The IMRT plan was computed using NOMOS CORVUS treatment planning system with five coplanar 4 MV beams. The MERT plan was computed using the modified EGS4/MCDOSE system with three coplanar beams (205^0, 235^0, and 255^0), with each beam being energy and intensity modulated. The final MERT dose distribution was computed based on intensity 15 maps reconstructed from corresponding 15 leaf sequences. The beamlet size is 1x1 cm for both plans. The isodose curves, normalized to 55 Gy, represent 10, 20, 30, 40, 50, 60, 70, 80, 90, and 100%, respectively. As shown here, the MERT plan offers at least similar or better target dose coverage and uniformity.
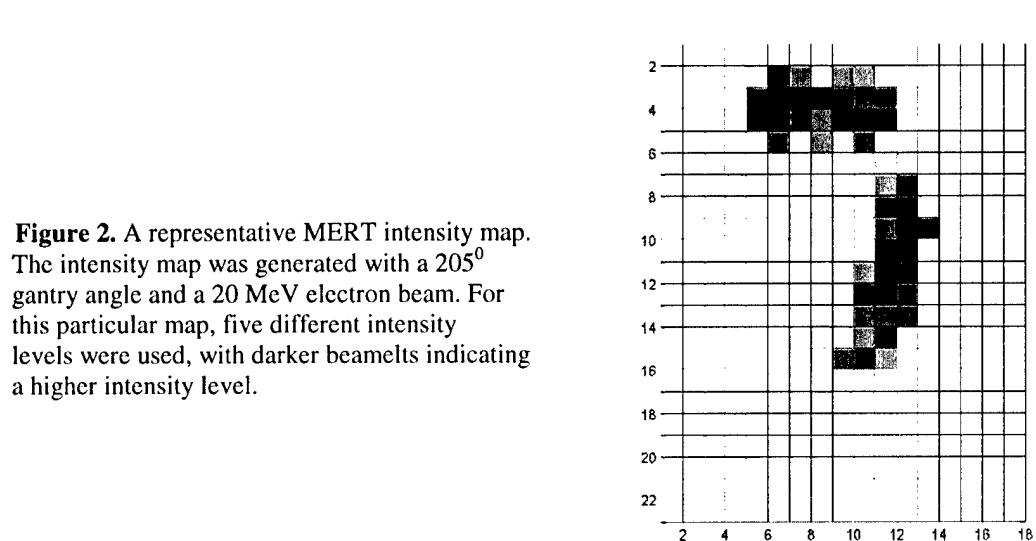
Figure 2. A representative MERT intensity map. The intensity map was generated with a 205^0 gantry angle and a 20 MeV electron beam. For this particular map, five different intensity levels were used, with darker beamelts indicating a higher intensity level.
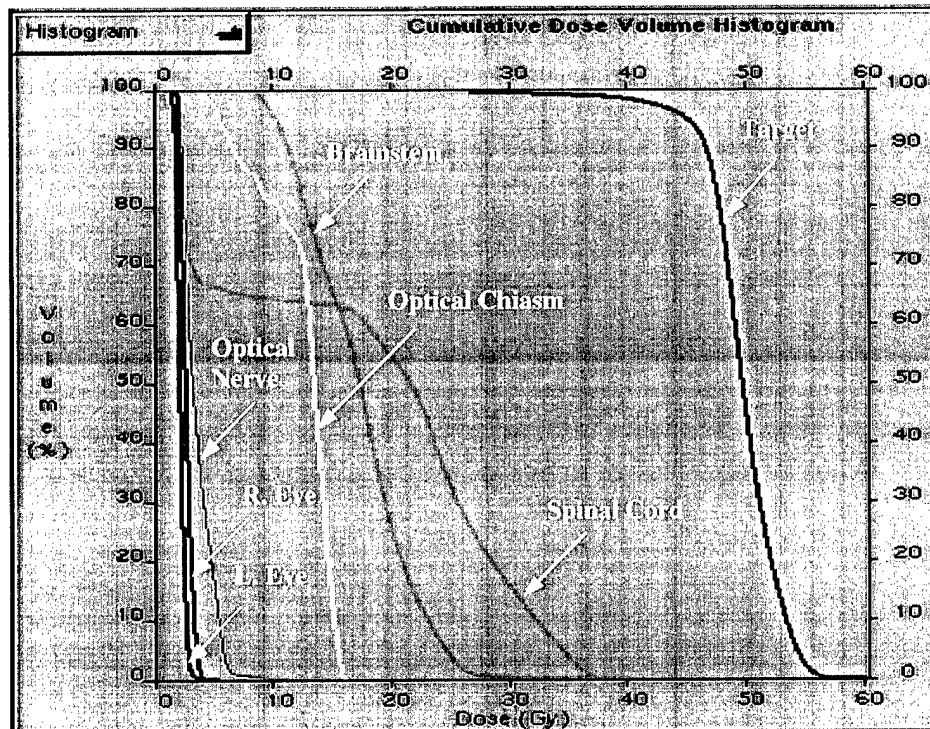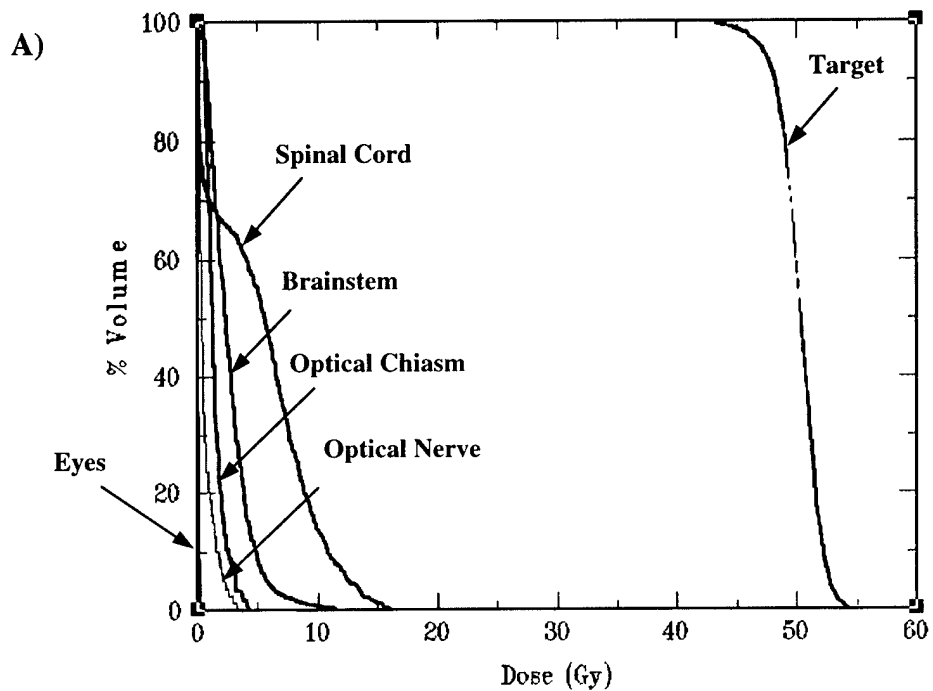
Figure 3. Comparison of dose volume histograms (DVH) for a representative head and neck case. **A)** DVH of the MERT plan. **B)** DVH of the corresponding IMRT plan. Clearly, the MERT plan shows superior normal tissue sparing.

Commissiong of Multigrid Superposition algorithm for IMRT treatment planning

Shahine B, Song Y, Findley D, Ma C-M, Boyer A, Pawlicki T
Department of Radiation Oncology, Stanford University School of Medicine, Stanford,
CA 94305, USA

Purpose/Objective: In photon radiation therapy, accurate three-dimensional dose computations using convolution/superposition algorithms have been extensively investigated. These are based on the idea of computing the dose by convolving the total energy released in the patient with Monte Carlo-generated energy deposition kernels. Current IMRT dose calculation algorithms are mostly based on Clarkson integration and pencil beam methods. The purpose of this study is the evaluation of FOCUS (Computerized Medical Systems, Inc., St. Louis, MO) Multigrid Superposition algorithm used as a dose calculation engine in intensity modulated radiation therapy treatment planning.

Materials & Methods: In FOCUS Multigrid superposition, the incident lateral fluence distribution of the accelerator is specified by the user. A fanned grid is created on which fluence and energy released in the patient is calculated. Kernels are represented in spherical coordinates and are allowed to change with the local electron density variations. Density scaling is used to distort the kernels to account for the effect of variations in electron density on the dose distributions. In commissiong FOCUS, we followed the recommendations of TG 53 for open field validation and density corrections (tissue inhomogeneities corrections) estimation in three dimensions. Several MLC shapes were constructed and comparison with film measurements was performed.

Results: Our results showed good comparison of central axis depth dose between FOCUS Multigrid Superposition and measurements to whitin 2%. Furthermore, isodose lines for 3x4 cm^2 and 5x5 cm^2 field sizes taken in axial planes were within 2 mm difference when compared with films. For MLC dose calculations, results of a circular field with 15 cm diameter were also within 2 mm of FOCUS calculations. Moreover, a C-shaped and a sinusoidal-shaped MLCs were employed and encouraging comparisons were obtained.

Conclusions: The importance of accurate dose calculations in IMRT treatment planning was addressed in this study. In head and neck cases where there is a definite need for accurate tissue inhomogeneity corrections, the FOCUS Multigrid Superposition algorithm was evaluated as a dose calculation engine for IMRT treatment planning. The agreement (measured vs. calculated) satisfied the Van Dyk criteria (IJROBP 26, 261-273, 1993) within the clinical range and within the inherent limitations of the algorithm.

A MULTILEAF COLLIMATOR FOR
MODULATED ELECTRON RADIATION THERAPY (MERT)
FOR BREAST CANCER

Yulin Song[1], Steve B. Jiang[2], Michael C. Lee[1], C-M Charlie Ma[3], and Arthur. L. Boyer[1]

Departments of Radiation Oncology,
[1]*Stanford University School of Medicine, Stanford, CA 94305*
[2]*Massachusetts General Hospital*
Harvard Medical School, Boston, MA 02114
[3]*Fox Chase Cancer Center, Philadelphia, PA 19111*

E-mail: yulin@reyes.stanford.edu

Results from recent clinical trials have shown that irradiation is an effective adjuvant therapy to lumpectomy, mastectomy, and chemotherapy for breast cancers of different stages. However, the conventional tangential photon beam treatment has two major limitations. Firstly, part of the lung and heart (in the case of the left breast treatment) may be exposed to high radiation dose. Secondly, the contralateral breast may receive a significant amount of scatter dose. Consequently, irradiation-related complications such as arm edema, myocardial infarction, severe breast fibrosis, and secondary breast cancer may occur in the patients who have undergone conventional photon beam treatment. To reduce radiation dose to normal structures and, thus, the complications, we have investigated treating breast cancers using modulated electron radiation therapy (MERT), making use of the rapid depth dose falloff characteristics of electron beams. To deliver MERT plans effectively, we designed and manufactured a prototype electron multileaf collimator (EMLC). The performance of the EMLC was experimentally evaluated and the results were compared with those of Monte Carlo simulations.

Based on the results of Monte Carlo simulations, an experimental EMLC was fabricated by modifying a conventional 25 x 25 cm^2 electron cone (Varian Medical Systems, Palo Alto, CA). The EMLC consisted of 30 steel leaf pairs, with each leaf being 0.476 cm wide, 20.0 cm long, and 2.54 cm thick. The maximum opening was 14.2 x 15.5 cm^2 when all leaves were completely retracted, giving the largest radiation field of 15.0 x 16.3 cm^2 projected at 100 cm source-surface distance (SSD). Film dosimetry was performed at energies of 6, 12, and 20 MeV in a solid water phantom to evaluate the quality of the electron beams collimated by the EMLC. Based on the manufacturer's specifications of the beam production system and the EMLC design, the electron beams were also simulated using the EGS4/BEAM code. MERT plans for breast cancer with five nominal energies (6, 9, 12, 16, and 20 MeV) were created using modified EGS4/MCDOSE code. The calculated doses were checked against a commercially available Monte Carlo dose calculation engine (NXEGS, NX Medical Software LLC, New York, NY) and measurements. The MERT plans were also compared with x-ray intensity-modulated radiation therapy (IMRT) in terms of target coverage and normal tissue sparing.

Our results showed that there was an excellent agreement between the film measurements and the Monte Carlo simulated data at all electron energies in terms of dose distribution. We found that the EMLC provided significant improvements in dose penumbras and field resolution as compared to the photon MLC. We also found that MERT was able to provide similar or better target dose coverage compared with x-ray IMRT. However, MERT could significantly reduce the dose to critical structures.

We conclude that EMLC was able to provide sufficient beam collimation for MERT and for superficial targets, such as breast cancers, MERT showed excellent target coverage and normal tissue sparing.

COMBINING ELECTRON WITH INTENSITY MODULATED PHOTON BEAMS FOR BREAST CANCER

Lei Xing[1], Jonathan G. Li[2], Yulin Song[1], David Y. Yang[1], Don Goffinet[1], and Arthur. L. Boyer[1]

Departments of Radiation Oncology,
[1]Stanford University School of Medicine, Stanford, CA 94305-5304
[2]University of Florida
Gainesville, FL 32610-0385

E-mail: lei@reyes.stanford.edu

Radiation therapy following removal of the tumor (lumpectomy) is accepted as an effective treatment modality in the management of both invasive and non-invasive breast cancer. Radiation therapy also plays an important role in the multi-modality management of locally advanced or inflammatory breast cancer as well as in the treatment for women with medial lesions and positive axillary nodes and those patients undergoing adjuvant bone marrow transplantation. With an increasing incidence of breast cancers and with the advantage of breast preservation, more women are choosing lumpectomy and radiation treatment as an alternative to mastectomy. In practice, however, there are many reports indicating undesired radiation effects in the intra-thoracic structures (such as the heart, lung and ribs) and risk of second cancers in the contra-lateral breast. A more effective radiation treatment method to reduce the dose to the sensitive structures is thus clinically important. In this work we report development of a breast cancer treatment technique using the combination of conventional electron beam(s) and intensity modulated photon beams.

In the stated treatment technique, an electron beam with appropriate energy was combined with 2 to 4 intensity modulated photon beams. An iterative algorithm was developed which optimizes the weight of the electron beam as well as the fluence profiles of the photon beams for a given patient. Three breast cancer patients with early-stage breast tumors were planned with the new technique and the results were compared with those from 3D planning using tangential fields as well as 9-field intensity-modulated radiotherapy (IMRT) techniques. The combined electron and IMRT plans showed better dose conformity to the target with significantly reduced dose to the ipsilateral lung, and in the case of the left-breast patient, reduced dose to the heart, than the tangential field plans. In both the right-sided and left-sided breast plans, the dose to other normal structures was similar to that from conventional plans and was significantly smaller than that from the 9-field IMRT plans. The optimized electron beam provided between 70% to 80% of the tumor dose at d_{max} of the electron beam.

In summary, the use of electron provides an effective method to limit the exit dose from the adjacent sensitive structures and the combined electron and IMRT technique showed significant improvement over the conventional treatment technique using tangential fields with markedly reduced dose to the ipsilateral lung and the heart. Optimization of the composite treatment may result in highly conformal radiation doses to the primary tumor target volume while significantly reducing doses to the normal structures and therefore minimizing side effects. This combination provides a unique opportunity to take advantage of the two types of radiation and to produce conformal dose distributions that would otherwise be impossible and has the potential to improve significantly the way that the breast cancer is treated and to avoid or greatly reduce the treatment complications and side effects.

Inclusion of biological parameter uncertainty in the treatment planning optimization

Yulin Song, Jun Lian, and Lei Xing
The Department of Radiation Oncology
Stanford University School of Medicine, Stanford, CA 94305

PURPOSE

Biological objective function for guiding dose optimization contains several biological parameters. Currently, radiobiology data are still sparse and of questionable quality. Whereas the general formalism remains the same, different sets of model parameters lead to obvious different solutions and thus critically determine the final plan. The purpose of this work is to describe an inverse planning formalism with inclusion of model parameter uncertainties.

MATERIALS AND METHODS

Two types of biological model based optimization were studied. The first one was defined as a product of TCP and a term associated with NTCPs of the involved structures. The second one is an equivalent uniform dose (EUD) based objective function. Here the EUD definition is used to illustrate the mathematical formulism. The parameter a in the EUD calculation is the tumor or normal tissue-specific parameter that describes the dose-volume effect. For convenience, we will use the concept of preference function. Assuming the uncertainty of a can be described by a Gaussian form distribution, for a given selected a^k, our preference over the occurrence of the EUD can be expressed as a conditional probability. The overall preference function can be obtained by summing a series of joint probabilities, each is a product of two preference functions corresponding to one permissible a. In this way, the uncertainty in a can be cast into the objective function or the preference function of the system based on Bayesian theorem. A mathematical phantom with a concave target and a circular organ at risk (OAR) is used for the assessment of the proposed algorithm.

RESULTS

Assuming that the desired dose parameter EUD_0 for the target, OAR and normal tissue are 72Gy, 35Gy and 35Gy, respectively, the change of EUD and preference function as a function of a is studied. Clinically acceptable plans are generated and compared when a is selected with pre-designed preference levels. The dose volume histograms (DVHs) show the uncertainty of the parameter has a profound impact of the inverse treatment planning optimization result. For illustration purpose, we have assumed that a could take three discrete values, -10, -50 and -5 with given probabilities. Figure 1 shows DVHs for two plans: solid curves correspond to the plan with fixed a while dotted curves correspond to the plan when a have three permissible values (a=-10 with 50% probability, -50 with 45% probability, and -5 with 5% probability). The target DVH is shifted to higher dose as expected and dose homogeneity is improved.

CONCLUSIONS

We have developed an inverse planning algorithm that allows us to include the uncertainties of biological model parameters into the dose optimization. Using this algorithm, the effects of the model parameter uncertainty can be minimized (in a statistical sense) and its influence on the final treatment can be more reliably predicted. This technique brings us a step closer towards our goal of individualizing radiotherapy treatment.
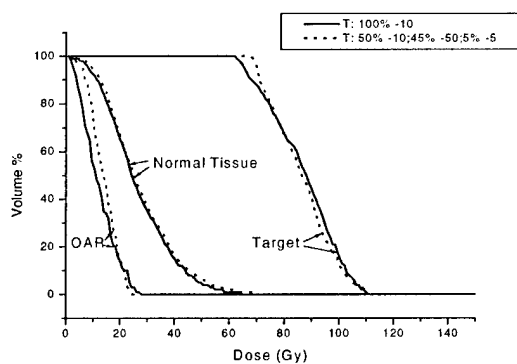
Fig. 1 Dose volume histograms (DVHs) when parameter a is fixed to one single value a=-10 (solid line) and when a is allowed to take three values (a=-10 with 50% probability, -50 with 45% probability, and -5 with 5% probability, dotted line).

AbstractID: 8116 Title: TLD measurement system for comprehensive dosimetric quality assurance in IMRT

TLD measurement system for comprehensive dosimetric quality assurance in IMRT

Intensity-modulated radiotherapy (IMRT) provides a technique for improving dose distributions by using inverse planning computer treatment plan optimization and computer-controlled dynamic delivery of complex planned intensity distributions. IMRT places unique demands on capabilities of treatment planning and delivery systems, strongly suggesting a need for a method of systematic quality assurance that includes detailed testing and verification of dose delivery. A multi-slab Plastic Water™ phantom was constructed to accommodate measurement in different planes of 2-D dose distributions from complete IMRT treatment plans with millimeter resolution, using 1-mm thermoluminescent dosimeter (TLD) cubes. The phantom can accommodate single-point ionization chamber measurement as well. The 30 x 30 cm axial cross section phantom was imaged with 1.5-mm spacing between CT slices, and the data set exported to a commercial IMRT treatment planning system (Corvus™) with an accompanying DICOM structure of idealized 30 x 30 axial contours to represent idealized surface anatomy. The planning system assigned the phantom a bulk density of that of water. Using Corvus utilities, clinical patient treatment plans were calculated as though they were applied to the slab phantom unchanged. Numerical data was extracted in matrix form from axial plane dose computation files by following a procedure documented by the manufacturer to convert dose images to 'tif' format, and a utility available within MATLAB™ software to interpret these files. Results were compared with TLD measurements. Initial data show general agreement of the shape of the calculated dose distributions, but with systematic relative deviations appearing in the lower-dose regions.

Dose profile: TLD vs. corvus, 15X, A-P, (avg 2 meas.)

(Ant to Post), cm
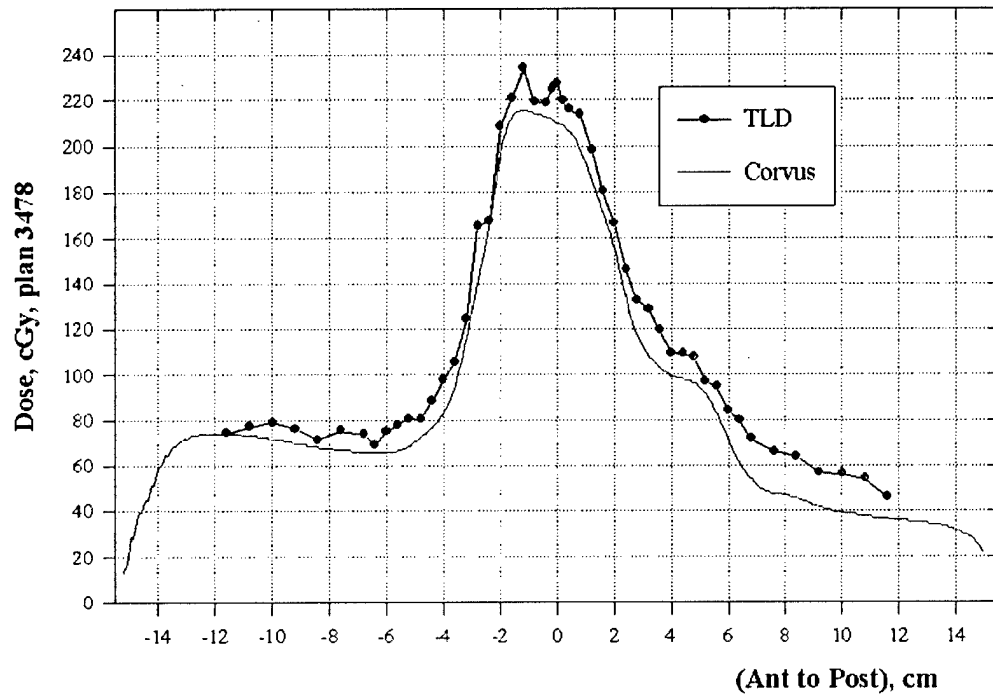
Small-field plan, 15X

Dose profile: TLD vs. corvus, 15X, RT-LT.(avg 2 meas.)

(RT to LT), cm